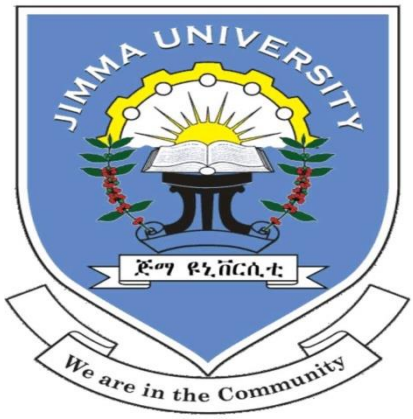

JIMMA UNIVERSITY

JIMMA INSTITUTE OF TECHNOLOGY

SCHOOL OF CHEMICAL ENGINEERING

GREEN SYNTHESIS OF ZINC OXIDE NANOPARTICLES AND ZINC OXIDE-SILVER NANOCOMPOSITES USING LEAF EXTRACT OF *BUDDLEJA POLYSTACHYA* (ANFAR) AND EVALUATION OF THEIR ANTIBACTERIAL ACTIVITY

By

Tsigab Tekleab

***Advisor*: Dr. Ramachandran Kasirajan (Ass. Professor)**

***Co-Advisor*: Mr. Mohammed Seid (MSc.)**

A thesis submitted to Jimma University, Jimma Institute of Technology, School of Chemical Engineering in partial fulfillment of the requirement of Masters of Science in Process Engineering.

March 2022

Jimma, Ethiopia

JIMMA UNIVERSITY

JIMMA INSTITUTE OF TECHNOLOGY

SCHOOL OF CHEMICAL ENGINEERING

GREEN SYNTHESIS OF ZINC OXIDE NANOPARTICLES AND ZINC OXIDE- SILVER NANOCOMPOSITES USING LEAF EXTRACT OF BUDDLEJA POLYSTACHYA (ANFAR) *AND EVALUATION OF THEIR ANTIBACTERIAL ACTIVITY*

By

Tsigab Tekle'Ab

***Advisor*: Dr. Ramachandran Kasirajan (Ass. Professor)**

***Co-Advisor*: Mr. Mohammed Seid (MSc.)**

A thesis submitted to Jimma University, Jimma Institute of Technology, School of Chemical Engineering in partial fulfillment of the requirement of Masters of Science in Process Engineering.

March 2022

Jimma, Ethiopia

Jimma University

Jimma Institute of Technology

School of Chemical Engineering

Process Engineering Program

As members of the examining committee of the final M.Sc. thesis open defense, this is to certify that the thesis prepared by Tsigab Tekleab entitled "*Green synthesis of Zinc oxide nanoparticles and Zinc oxide-Silver nanocomposites using leaf extract of Buddleja Polystachya (*Anfar*) and evaluation of their antibacterial activity*" complies with the regulations of the university and meets the accepted requirements for the degree of Master of Science in Chemical Engineering (Process Engineering).

Approved by the Examining Committee:

Dr. Ramachandran Kasirajan (Ass. Professor)	_____	_____
Advisor	*Signature*	*Date*
Dr. Shimelis Kebede (Ass. Professor)	_____	_____
External Examiner	*Signature*	*Date*
Mr. Temesgen Abeto (MSc.)	_____	_____
Internal Examiner	*Signature*	*Date*
Mr. Ermias Girma (Ass. Professor)	_____	_____
School Dean	*Signature*	*Date*
Ms. Ebise Getacho (MSc.)	_____	_____
Chair Person	*Signature*	*Date*

DECLARATION

I, the undersigned, declare that this thesis entitled "*Green synthesis of Zinc oxide nanoparticles and Zinc oxide-Silver nanocomposites using leaf extract of Buddleja Polystachya (*Anfar*) and evaluation of their antibacterial activity*" is my original work with the guidance of my advisors, and has not been presented by any other person for an award of a degree in Jimma University or any other University, and that all resources of materials used for this study have been duly acknowledged.

Name

Tsigab Tekleab	_____	_____
	Signature	*Date*

This MSc. thesis has been submitted for examination with the approval of thesis advisors and program coordinator.

Dr. Ramachandran K. (Ass. Professor)	_____	_____
Advisor Name	*Signature*	*Date*
Mr. Mohammed Seid (MSc.)	_____	_____
Co-Advisor Name	*Signature*	*Date*
Mr. Ketema Beyecha (MSc.)	_____	_____
Program Coordinator	*Signature*	*Date*

ACKNOWLEDGEMENT

First of all, I would like to give glory to the almighty God, for the infinity of goodness, from whom every good gift comes, for the gifts of health and patience from the beginning to the end of this thesis work and in every moment of my life.

Next, my sincere gratitude and earnest appreciation go to my advisor Dr. Ramachandran Kasirajan and Co-advisor Mr. Mohammed Seid for their guidance, advice, patience, and encouragement upon preparation of this thesis. Furthermore, I would like to thank all staff members of the School of Chemical Engineering for sharing their helpful knowledge and experience.

I would also like to thank all laboratory staff of the School of Chemical Engineering and School of Material Sciences and Engineering, especially Mr. Defar Getahun and Mr. Tsegaye Markos for their endless support throughout the experimental work. Moreover, I would like to thank all lab technicians of the Chemistry and Biology departments of Jimma University and Chemical Engineering of Addis Ababa Science and Technology University.

Finally, I have no words to express thanks to my Loving Parents, as my entire personality to this stage is the result of their efforts, prayers, inspiring response, and encouragement throughout my life.

ABSTRACT

In this study, pure eco-friendly plant extract of Buddleja Polystachya (Anfar), zinc acetate ($Zn(CH_3COO)_2$) as host, and silver nitrate ($AgNO_3$) as dopant precursors were used to synthesize zinc oxide (ZnO) nanoparticles and zinc oxide–silver (ZnO–Ag) nanocomposites. The synthesis condition of ZnO-Ag nanocomposites was optimized using a central composite design (CCD). Temperature (Temp), pH, and $AgNO_3$ solution concentration (Conc. Ag) were used as independent variables in the model, while absorbance intensity of the nanocomposite was used as the dependent variable.The prepared nanoparticles and nanocomposites were characterized by using various analytical and spectroscopic tools such as UV-visible spectroscopy, Fourier Transform Infrared Spectroscopy, powder X-ray diffraction, and Dynamic Light Scattering. Along with this study, the antibacterial activity of the biosynthesized ZnO-NPs and ZnO–Ag NCs was investigated against Streptococcus aureus and Escherichia coli. The phytochemical analysis revealed that tannins, steroids, phlobatanins, saponins flavonoid, phenols and terpenoids are the major chemical constituents of the extracts obtained from B.polystachya leaf extracts. The predicted optimal synthesis condition ZnO-Ag NCs was found to be Temperature = 53.709 °C, pH = 8.794, and Conc.Ag= 91.454 mM with maximum absorbance intensity of 1.951. *The UV-visible spectroscopy result shows that, the maximum absorbance intensity of ZnO NPs and ZnO-Ag NCs were found to be 2.073 and 1.905 respectively. Moreover, the bandgap energy was found as 3.31 eV and 3.28 eV for ZnO NPs and ZnO-Ag NCs, respectively. The XRD analysis revealed that the average crystallite size was discovered to be 24.50 and 23.55 nm for ZnO and ZnO–Ag nanoparticles, respectively. According to dynamic light scattering results, the average size of ZnO NPs and ZnO-Ag NCs was 78.69 nm and 35.48 nm, respectively, indicating that the nanomaterials were successfully formed. Finally, the antibacterial activity results showed that ZnO-Ag NCs displayed higher activity against the bacterial strains compared with pure ZnO NPs with the maximum zone of inhibition 15 ± 0.31 and 8 ± 0.37 mm for E. coli and, S.aureus respectively. As a result, this study reports a rapid and environmentally friendly path for the synthesis of ZnO NPs and ZnO-Ag NCs with moderate antibacterial activity.*

***Keywords**: Buddleja Polystachya, Green synthesis, ZnO nanoparticles, ZnO-Ag nanocomposites, Antibacterial activities*

TABLE OF CONTENTS

LIST OF TABLES

LIST OF FIGURES

LIST OF ABBREVIATIONS AND ACRONYMS

ANOVA	Analysis of variance
ASTM	American Society of Testing and Materials
BAuA	Bundesanstalt für Arbeitsschutz und Arbeitsmedizin.
B.Polystachya	Buddleja Polystachya
BSI	British Standards Institution
CCD	Central composite design
Conc.	Concentration
CVD	Chemical vapor deposition
DLS	Dynamic light scattering
E.coli	Escherichia coli
FTIR	Fourier transform infrared
FWHM	Full width at half maximum
ISO	International Organization for Standardization
NCs	Nano composites
NIOSH	National Institute of Occupational Safety and Health
NPs	Nano Particles
PDI	Polydispersity index
PL	Photoluminescence
PVD	Physical vapor deposition
RSM	Response surface methodology
SCCP	Scientific Committee on Consumer Product
S.aureus	Staphylococcus aureus
Temp.	Temperature
UV	Ultraviolet
UV-Vis	Ultraviolet visible spectroscopy
XRD	X-ray Diffraction

1. INTRODUCTION

1.1 Background of the Study

Nanotechnology is a fast expanding discipline with applications in various fields of science and technology for the creation of novel nanoscale materials (Sharmila & Gayathri, 2014). Because of its importance and applications, research and development in nanoscience have been grown throughout the world during a short period. The introduction of new types of nanomaterials, such as nanofilms, nanoparticles, nanowires, and nanoclusters, is one of the key outcomes of these investigations (Nikaeen *et al*., 2020). Metal oxide nanoparticles (MONPs) are interesting among nanomaterials because of their excellent optical, chemical, electrical, and magnetic capabilities. These properties bring the materials interesting in different application areas, including nanoelectronics devices, catalysis, nonlinear optical devices, bio-medical, etc. (M. Zare *et al*., 2018).

Nowadays, between metal and metal oxides, zinc oxide (ZnO) and silver (Ag) nanoparticles have gotten large attention. This is because that ZnO has a wide-band gap, great chemical stability, large surface area, and low cost with various applications, including use in solar cells, electronics, sensors, and photo electronics. Similarly, Ag nanomaterials illustrate some unique properties in chemical and biological sensing and high electrical conductivity (M. Zare *et al*., 2018). Due to their new effects on the evolution of antibacterial activity and efficiency of photo catalytic activity of semiconductors, Ag ions have recently attracted the attention of various research projects (Dumbrava *et al*., 2019). ZnO nanoparticles (NPs), on the other hand, have recently gotten high attention because they have a vast range of properties that are dependent on doping, including a wide range of conductivity from metallic to insulating, high transparency, a large bandgap, wide binding energy, semi-conductivity, and a high melting point (Gurgur *et al*., 2020).

So far several various NPs synthesis methodologies such as chemical methods, electro-chemical methods, photochemical methods, gamma radiation methods, and laser ablation techniques have all been used to synthesize nanoparticles. One of the greatest impediments to the use of most of these traditional processes in nano-production is their high cost, as well as the fact that some of them involve hazardous solvents and synthetic reactants that are damaging to the environment

(Dinah *et al*., 2019). As a result, scientists have recently grown interested in employing plant extracts and microorganisms to create green nanoparticles (Gunnarsson *et al*., 2016).

Unlike the conventional methods, green nanotechnology makes use of environmentally friendly resources that are inexpensive or free. This process produces nanoparticles that are usually stable, hydrophilic, and have a very small diameter. Furthermore, plant extract precursors contain a wide range of active substances that aid in the reducing and stabilizing process as well as serve as templates for nanostructure manipulation (Dinah *et al*., 2019). According to Gunnarsson *et al*. (2016), biosynthesizing precursors are not only safe to handle, but the process also scales up quickly without the use of energy, high temperatures, or hazardous reagents, making it a more environmentally friendly option to physical and chemical syntheses.

Buddleja Polystachya (*B.polystachya*) leaf extracts were selected for the synthesis of ZnO NPs and ZnO-Ag nanocomposites (NCs) in this study since it is the first report on the plant being used for green nanoparticle synthesis. *B.polystachya* is an endemic medicinal plant found in the semi-arid highlands surrounding the Red Sea in Saudi Arabia, Yemen, Somalia, Ethiopia, and Eritrea, where it grows in secondary brush or around a forest, frequently alongside watercourses. Ethiopian traditional medicine uses *B.polystachya* leaves to treat a range of skin conditions (Houghton, 1984).

In this study, phytochemical constituents of *B.polystachya* leaves were extracted and the presence of several reducing, stabilizing, and capping agents in the leaf extract were performed qulitativeley using standard methods of phytochemical screening. ZnO NPs and ZnO-Ag NCs were synthesized in an environmentally friendly manner using Zinc acetate dihydrate ($Zn(CH_3COO)_2.2H_2O$) as host and silver nitrate ($AgNO_3$) as dopant precursors and leaf extract of *B.polystachya*. Here also, the influence of different experimental variables such as reaction temperature, pH, and concentration of $AgNO_3$ solution was studied using response surface methodology (RSM). The RSM is a statistical and mathematical method that is frequently used to investigate multiple regression analysis using quantitative data gathered from relevant experiments to discover and solve multivariant equations simultaneously.

Different optical and structural characteristics of the synthesized nanomaterials are also characterized using advanced techniques such as UV-visible spectroscopy, Fourier Transform

Infrared Spectroscopy, powder X-ray diffraction, and Dynamic Light Scattering. Furthermore, the antibacterial activity profile of the biosynthesized nanomaterials against two bacterial strains was investigated.

1.2 Statement of the Problem

Antibiotic resistance among bacteria is currently at an all-time high, and it is the world's major public health issue in the treatment of human patients with infectious diseases. Bacterial pathogens such as *S.aureus* and *E.coli* have acquired drug resistance genes, making them resistant to numerous antibacterial medicines. The main mechanisms whereby the bacteria develop resistance genes to antimicrobial agents include enzymatic inactivation, modification of the drug target(s), and reduction of intracellular drug concentration by changes in membrane permeability or by the overexpression of efflux pumps (Handzlik *et al*., 2018). Due to the various mechanisms, multidrug-resistant human pathogenic microorganisms are posing a growing threat to the medical community. However, the increasing resistance of diverse pathogenic organisms to various antibiotics has prompted a wide range of studies into alternate therapeutic options. Particularly, inorganic nanomaterials, such as metal oxide nanoparticles, are gaining interest in exploring various options to address this problem. Among metal oxide nanoparticles, ZnO NPs and their NCs have advantages over common organic and antibiotic compounds since they have lower toxicity, greater durability, and higher stability and selectivity. To produce such nanoparticles, green synthesis using plant extracts is one of the most important areas for the development of novel antibacterial drugs. Thus, *B.polystachya* leaf extract was utilized in this study to synthesize ZnO NPs and ZnO-Ag NCs using a green synthesis method, and their antibacterial activity was evaluated.

Even though various research studies have been conducted on the synthesis of ZnO NPs for antibacterial applications, green nanoparticle synthesis using indigenous plant extracts is not widely practiced. Furthermore, no comparative study of green synthesized ZnO NPs and ZnO-Ag NCs against human pathogenic bacteria using *B.polystachya* plant extract as a reducing agent has been published yet. Ethiopia, on the other hand, is home to diverse agro ecology and flora of many medicinal plants, the majority of which have remained unexploited and traditionally used. *B.polystachya* is among these most useful plants which are not well known about its valuable uses and so far its many uses are not discovered.

Therefore, this research is intended to fill the gap in the area of green synthesis of ZnO NPs and ZnO-Ag NCs from the leaves of *B.polystachya* and to investigate and compare their effect against two bacterial strains *Staphylococcus aureus* (gram-positive) and *Escherichia coli* (gram-negative).

1.3 Objectives of the Study

1.3.1 General Objective

The general objective of this study was green synthesis, optimization, and characterization of ZnO NPs and ZnO-Ag NCs using leaf extract of *B.polystachya* and evaluation of their antibacterial activity.

1.3.2 Specific Objectives

- To analyze the phytochemical screening of the leaf extract of *B.polystachya*.
- To synthesize ZnO NPs and ZnO-Ag NCs using leaf extract of *B.polystachya* and the precursor salt zinc acetate dihydrate and $AgNO_3$ as a dopant.
- To study the effect of reaction temperature, pH, and concentration of $AgNO_3$ salt on the synthesis of Ag-ZnO NCs using RSM.
- To characterize the synthesized ZnO NPs and Ag-ZnO NCs using UV-Vis, XRD, FT-IR, and DLS.
- To evaluate and compare the antibacterial activity of the synthesized ZnO NPs and Ag-ZnO NCs.

1.4 Significance of the Study

This study is expected to have its contribution to the area of green nanotechnology: green synthesis of the ZnO NPs and ZnO-Ag NCs using locally available *B.polystachya* extracts. It is also believed that it will have significance on creating a positive impact on increasing the number of available research works related to the synthesis of ZnO NPs and ZnO-Ag NCs using the indigenous plant and effective antibacterial activity. Having easily available ZnO NPs and ZnO-Ag NCs are also expected to overcome the increasing bacterial resistance of antibiotics to keep people healthy. Moreover, this study is expected to be used as one possible means of plant-mediated synthesis of pure ZnO NPs with low cost, eco-friendliness, and convenient methods of preparation to avoid the toxicity and hazardous of those synthesized by chemical methods. Thus, it will pave a way for

technology transfer and further explorations on many Ethiopian indigenous plants used for antibacterial applications.

1.5 Scope of the Study

The scope of this study was limited to the green synthesis and optimization of ZnO NPs and ZnO-Ag NCs using plant extracts of *B.polystachya* leaves and their characterization using, UV, XRD, FT-IR, and DLS techniques. Besides the antibacterial activity of the biosynthesized nanomaterials against gram-positive bacteria (*staphylococcus aureus*) and gram-negative bacteria (*Escherichia coli*) was evaluated and compared.

1.6 Limitation of the Study

With the objective in mind, certain limitations are defined to set the scope of this study. The major constraint was the failure of characterizing instruments during the experimental season. Due to that, this study does not perform the thermogravimetric analysis (TGA) of ZnO NPs and ZnO-Ag NCs that determines their thermal stability and decomposition. Furthermore, although, the shape and size of the nanomaterials are determined using X-ray diffraction (XRD) and dynamic light scattering (DLS), this study does not further confirm their morphology using a scanning electron microscope (SEM). Moreover, due to similar reasons, this study does not perform the elemental analysis of ZnO-Ag NCs using Energy-dispersive X-ray spectroscopy (EDS).

2. LITERATURE REVIEW

2.1 Background

Particulate dispersions or solid particles with a size in at least one dimension in the range of 10-100nm are defined as nanoparticles. A nanoparticle is the most basic component in the fabrication of a nanostructure, and it is much smaller than the world of everyday objects described by Newton's laws of motion but much larger than an atom or a simple molecule governed by quantum mechanics (Mohanraj & Chen, 2006).

As Horikoshi & Serpone (2013) state, metallic nanoparticles differ from bulk metals in terms of physical and chemical properties (e.g., lower melting points, higher specific surface areas, specific optical properties, mechanical strengths, and specific magnetizations), which could be useful in a variety of industrial applications. The way a nanoparticle is viewed and defined, on the other hand, is highly dependent on the application. Table 1.1 summarizes the various organizations' definitions of nanoparticles and nanomaterials in this regard.

Table 2.1 Definitions of nanoparticles by different organizations

Organization	Definition of nanoparticle
ISO	A particle with a diameter of 1–100 nm.
ASTM	An ultrafine particle with a length of 1–100 nm in two or three spots.
NIOSH	A particle with a diameter of 1–100 nm, or a fiber with a diameter of 1–100 nm.
SCCP	At least one of the sides is nanoscale.
BSI	The fields and sizes are all in the nanoscale.
BAuA	The fields and sizes are all in the nanoscale.

(Source: Horikoshi & Serpone, 2013)

Nanocomposites, on the other hand, are composites in which at least one of the phases has dimensions in the nanometre range. Nanocomposite materials have emerged as viable alternatives to micro composites' baffling limitations. They have also been dubbed "21st-century resources" because of their design rarity and property groupings that are not found in traditional composites. Nanocomposites have a vast range of potential applications, including optical communications,

electronics, and biological systems, as well as new materials. Many potential applications have been investigated, as well as numerous devices and systems (Din *et al*., 2019).

Nanoparticle synthesis techniques can be divided into two categories: top-down and bottom-up. Atoms and molecules are used as building blocks in the bottom-up approach to synthesizing complex nanostructures. Top-down approaches rely on bulk particle miniaturization to create desired nanostructures with various properties. Both methods can be used in nanostructure engineering to determine the shape, size, and properties of nanoparticles for a specific application. Physical, chemical, and biological synthesis approaches are also classified based on the processes or materials used in the manufacturing process (Jeevanandam *et al*., 2016).

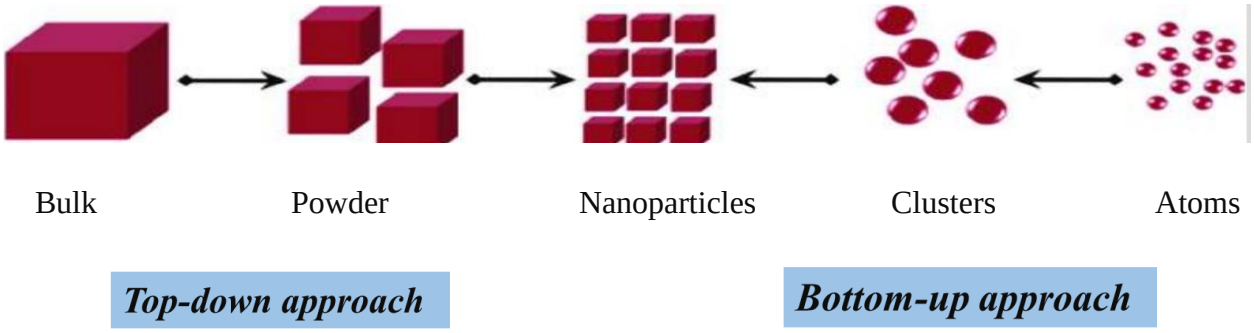

(Source: Patra & Baek, 2014)

Figure 2.1 Techniques for synthesis of nanoparticles

2.2 Methods of Nanoparticle Synthesis

Metal oxide nanoparticle synthesis methods are divided into physical, chemical, and biological approaches (J. Singh *et al*., 2018).

2.2.1 Physical methods

The physical method is a conventional method of nanoparticle synthesis that uses a "top-down" strategy in which the bulk material is pulverized into fine particle matter through force applied, such as impact, crushing, disruption, cutting, degradation, grinding, processing and homogenization. In micro-particle fracturing, physical procedures such as milling are employed, and a few instances include mechanical milling, physical vapor deposition (PVD), and sputtering (Bipin & Art, 2020). Mechanical milling is a top-down process in which powdered particles are repeatedly deformed, resulting in a dramatic reduction in particle size and the formation of

nanostructures. PVD involves converting a solid bulk material into a gaseous state and then cooling it under a vacuum to allow for the re-deposition of particulates in nanoscale dimensions. Sputtering, on the other hand, uses high-energy ions to knock atoms or molecules from a target, which acts as one electrode and deposit them on a substrate, which acts as the other electrode. Physical synthesis methods are extremely useful for creating ultra-thin, ultra-pure nanostructures and nano-alloys (Yadav *et al*., 2012). These technologies, on the other hand, are versatile in that they can produce nanoparticles of higher size, diameter, and volume that are still regulated, but they produce surface flaws, contamination, and are expensive and time-consuming. It may also be possible to make nanoparticles of the same size, but instrument assembly and maintenance are prohibitively expensive (Bipin & Art, 2020).

2.2.2 Chemical methods

Chemical synthesis is the process of creating nanoparticles by forming ions through a series of chemical reactions. Some of the most common chemical methods for nanoparticle synthesis include chemical vapor deposition (CVD), sol-gel, liquid phase method, colloidal method, and electrode-position (Kartopu & Yalçın, 2010).

CVD is similar to physical vapor deposition, but it involves the use of catalysts to speed up chemical reactions. Nanoparticles can be prepared using CVD processes for microelectronics, optoelectronics, protective, decorative, and optical coatings. The reaction of molecular precursors in an aqueous solution or non-aqueous solvent is known as liquid phase chemical synthesis. These precursors react to form unstable solutions, which are then nucleated, resulting in the synthesis of homogeneous or heterogeneous nanoparticles. The sol-gel process employs a series of chemical reactions that transform a homogeneous solution of molecular reactant precursors (a sol) into an infinite three-dimensional polymer (a gel), resulting in an elastic solid that fills the same volume as the solution. Colloidal synthesis, on the other hand, is a relatively simple, inexpensive, and widely used method for producing metal and semiconductor nanocrystals. Electrodeposition is a technique for the synthesis of nanoparticles that uses voltage to induce chemical reactions in aqueous solutions. Nanowires, nano-porous materials, and nanocylinders have all been created using this method (Jeevanandam *et al*., 2016).

2.2.3 Limitation of conventional methods

Physical and chemical synthesis methods have produced promising results with various morphologies of nanoparticles for various applications, but they are still costly and require the utilization of hazardous chemicals. Furthermore, when they are exposed to real-world/specific applications, they may face the following limitations or challenges: (J. Singh *et al*., 2018)

(i) Stability in a hostile environment,
(ii) Lack of awareness in fundamental methodology and modeling factors,
(iii) Bioaccumulation/toxicity features,
(iv) Extensive analysis requirements,
(v) Need for skilled operators,
(vi) Device assembly and structure problems, and
(vii) Recycle/reuse/regeneration.

2.2.4 Biological synthesis of nanoparticles

To counteract the limitations of traditional methods, a new era of "green synthesis" techniques is gaining traction in current materials science and technology research and development. Green nanomaterial synthesis, as a result of legislation, control, cleanup, and remediation, will directly contribute to their environmental friendliness. Several components, such as waste prevention/minimization, derivatives/pollution reduction, and the use of safer (or non-toxic) solvents/auxiliaries, as well as renewable feedstock, can thus explain some basic principles of "green synthesis." (J. Singh *et al*., 2018).

These green strategies use natural biological agents that are ecofriendly, biodegradable as reducing, capping, and stabilizing agents for nanoparticle syntheses like plants, microbes, and enzymes that are regarded as non-hazardous to humans (Bipin & Art, 2020).

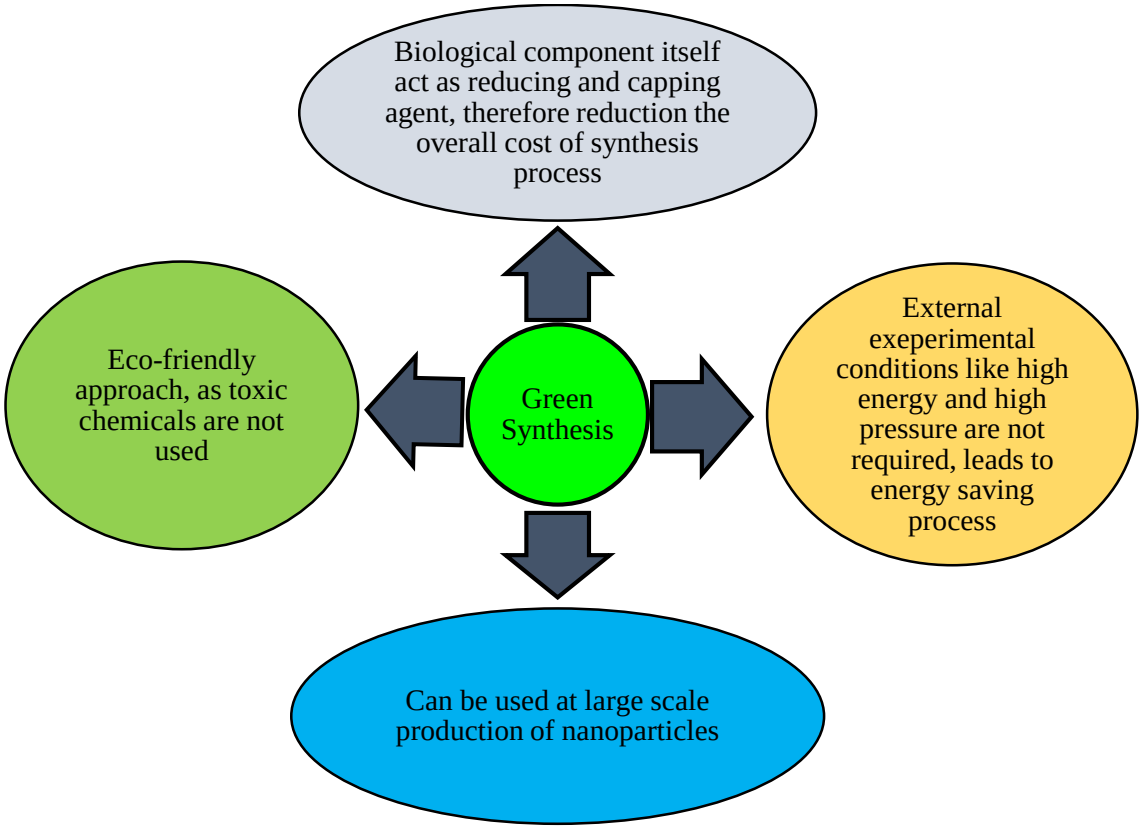

(Source: Singh *et al*., 2018)

Figure 2.2 Key merits of green synthesis

2.2.4.1 Microbial Synthesis of Nanoparticles

Microorganisms such as fungi, bacteria, yeast, and algae have all been identified as potential sources for the synthesis of metal oxide nanoparticles. While algae are still being researched, bacteria and fungi are the most common and widely used microbes so far.

Commercial biotechnological applications such as bioremediation, genetic engineering, and bioleaching have all made use of bacterial species. Bacteria have remarkable abilities to reduce heavy metal ions and could be used to create nanoparticles (Jeevanandam *et al*., 2016). Different bacterial species were used to synthesize metal, metal oxide, and other new nanoparticles, according to Singh *et al*. (2018). Metal and metal oxide nanoparticles have been widely synthesized using prokaryotic bacteria and actinomycetes.

Fungi are also regarded as a good biological agent for metal and metal sulfide NPs synthesis due to the diversity of their intracellular enzymes. Fungi, in comparison to bacteria, can produce more

nanoparticles. The use of fungal biomass in the production of metal, metal oxide, and other novel nanoparticles has been reported (J. Singh *et al*., 2018).

2.2.4.2 Plant-Mediated Synthesis of Nanoparticles

Metal ion reduction takes longer in fungi and bacteria, but water-soluble phytochemicals can reduce metal ions in a fraction of the time. Plant-mediated extracts, on the other hand, are an excellent source of metal and metal oxide nanoparticle synthesis due to the presence of several easily extracted phytochemicals (Jeevanandam *et al*., 2016). Phytochemicals can be found in a variety of plant parts, including leaves, seeds, barks, roots, and fruits. Leaf extracts, on the other hand, are high in bioactive compounds like alkaloids, amino acids, alcoholic compounds, and various chelating proteins, all of which are thought to be responsible for the reduction of metal ions into nanoparticles. As a result, they are a good source for nanoparticle biosynthesis (Shafey, 2020).

Furthermore, plant leaf extracts are thought to act as both reducing and stabilizing agents in the synthesis of nanoparticles. Because different leaf extracts contain varying concentrations of biochemical reducing agents, the composition of the leaf extract has an impact on nanoparticle synthesis. Terpenoids, ketones, flavonoids, amides, aldehydes, and carboxylic acids are the main phytochemical components involved in the biosynthesis of nanoparticles (Jeevanandam *et al*., 2016).

In general, the utilization of plant extracts in a simple, ecofriendly, and easy process to synthesis NPs at a large scale is preferred over bacteria and/or fungi-mediated synthesis among the various green metal and metal oxide nanoparticle production methods (J. Singh *et al*., 2018). The synthesis of metal oxide NPs using plant extracts is also a very cost-effective method, according to Hemalatha & Makeswari (2017) when compared to other physical and chemical methods. As a result, plant-mediated metal oxide nanoparticle synthesis is a hot topic right now.

Plant cultures, on the other hand, can only biosynthesis nanoparticles under specific conditions. The main influencing factors in plant extract-mediated synthesis are temperature, pH, and salt concentrations (Jeevanandam *et al*., 2016).

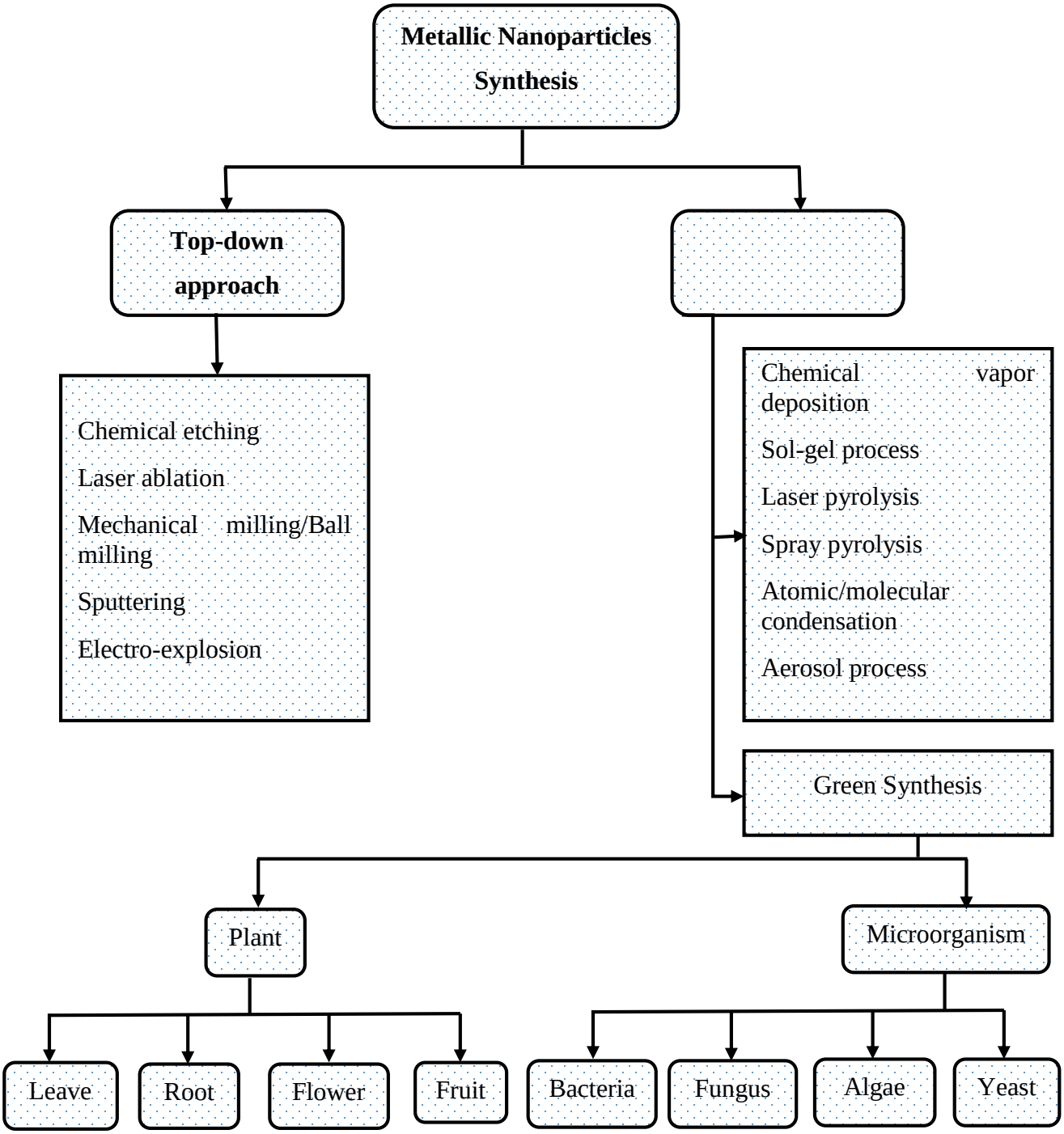

(Source: J. Singh *et al*., 2018)

Figure 2.3 Different synthesis approaches available for the preparation of metal nanoparticles.

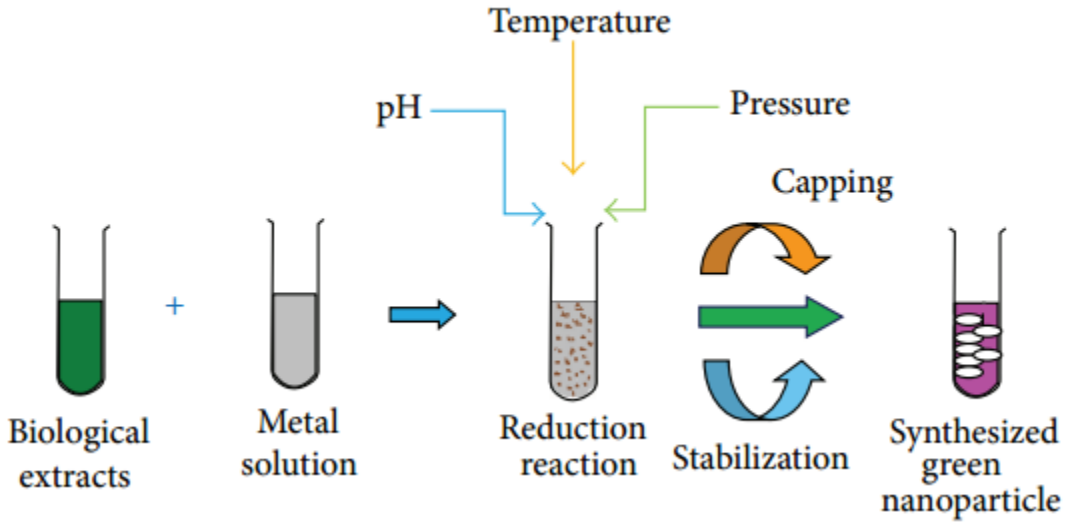

(Source: Patra & Baek, 2014)

Figure 2.4 Biological synthesis of nanoparticles using green technology

2.3 Factors Affecting the Synthesis of Green Nanoparticles

The synthesis, characterization, and application of nanoparticles are all influenced by a number of factors. The reaction temperature, pH of the solution, the concentration of the extracts used, and concentration of the raw materials utilized, size, and, most importantly, the protocols followed for the synthesis techniques used all have an impact on nanoparticle synthesis (Patra & Baek, 2014). The following are some of the most important factors that influence nanoparticle biosynthesis.

2.3.1 Reactant Concentration

The size, shape, and morphology of nanoparticles are influenced by metal ion concentration and bimolecular concentration in plant extracts (Forruque *et al*., 2021). Because nanoparticles are so small that they cannot be seen with the naked eye, it is advisable to use a reactant salt concentration in the range of 0.1–100 mM or even higher concentrations. As a result, only a minimal amount of the reactant is required for the reaction to take place. The reduction of the metal ion will not be successful if the reactant concentration is raised, and buildup may occur (Bipin & Art, 2020). In fact, using greater concentrations for nanoscale particle production makes no sense. The amount of leaf extract, or the volume of leaf extract, influences nanoparticle processing and the time necessary for nanoparticle creation (Bipin & Art, 2020). The efficacy of nanoparticle synthesis is frequently determined by the concentration of plant extract. Several studies have found that

increasing the proportion of plant extract in biomass dose enhances nanoparticle production while also changing their shape (Jameel *et al*., 2020).

2.3.2 pH

The pH of the solution influences the size, shape, and rate of synthesis in the plant-mediated biosynthesis of nanoparticles. The ability of the reaction (pH) to vary the electrical loads of biomolecules, which may affect their ability to cap and stabilize, and, as a result, the formation of nanoparticles, is a major influence (Bipin & Art, 2020). This influence is attributed to an increase in the development of nucleation centers as pH increases. The metal ions reduction to metal nanoparticles increases concomitantly with the expansion of the nucleation center that could be affected by changing pH. Furthermore, the pH of the solution regulates the activity of the functional groups in the plant extract, which dictates the metal salt reduction rate (Jameel *et al*., 2020). According to Patra & Baek (2014), the morphology and size of synthesized nanoparticles are influenced by the solution pH. As a result, changing the pH of the solution media can control nanoparticle size.

2.3.3 Reaction Temperature

The size, shape, and synthesis rate of nanoparticles are all influenced by the reaction temperature (Jameel *et al*., 2020). The physical method necessitates the highest temperature (>350°C), whereas chemical methods necessitate a lower temperature (below 350°C). In most cases, green technology nanoparticle synthesis necessitates temperatures of less than 100°C or room temperature. The temperature of the reaction medium determines also the nature of the nanoparticle generated (Patra & Baek, 2014).

2.3.4 Reaction Time

The duration of reaction/incubation of the suspension also significantly affects the size, shape, and degree of nanoparticles synthesized using plant-based biomaterials (Jameel *et al*., 2020). Similarly, the properties of synthesized nanoparticles changed over time and were heavily influenced by the synthesis process, light exposure, storage conditions, and other factors (Bipin & Art, 2020). Variations in time can occur in a variety of ways, including particle aggregation as a result of long-term storage; particles may shrink or grow as a result of long-term storage; they may have a shelf life, and so on, all of which affect their potential (Patra & Baek, 2014).

2.4 Zinc Oxide Nanoparticles and Silver-Zinc Oxide Nanocomposites

2.4.1 Zinc oxide nanoparticles

ZnO is the most promising inorganic oxide, with magnetic, electrical, and optical properties that make it widely used. Electronics, optoelectronics, and laser technology all benefit from their appealing properties at room temperature and pressure. ZnO NPs are currently being used in light-emitting devices, solar cells, biosensors, and photocatalysis. ZnO is a biocompatible oxide semiconductor that is also a low-cost luminescent material (Elmineh, 2019).

ZnO is abundant in three forms as a semiconductor: hexagonal wurtzite, rock salt, and cubic structures. Wurtzite, for example, has a direct bandgap energy of 3.40 EV (Sarah *et al*., 2019), making it transparent in the visible region but active in the UV/blue. Furthermore, ZnO's conductivity and luminescence improve optical absorption and UV filtering properties, resulting in ZnO NPs' advanced biosensing ability (Kalpana & Rajeswari, 2018). ZnO is non-toxic and has a large surface area-to-volume ratio in its nanoparticles.

ZnO NPs are employed in a variety of applications such as light-emitting diodes, drug delivery, solar cells, photocatalytic degradation, metal-insulator-semiconductor diodes, and personal care products due to their unique electrical, chemical, and optical properties, making them the most feasible, economically viable, and time-efficient approach because the chemicals are less harmful to the environment (Demissie *et al*., 2020).

2.4.2 Zinc oxide-Silver nanocomposites

ZnO NPs offer a wide range of biological uses since they are biocompatible, have a short survival time in the body, and can be dissociated and absorbed quickly. ZnO, on the other hand, has a slow photocatalytic decomposition rate, and adding metal ions can boost its activity. As a result, it's intriguing to see if forming nanocomposites with other materials, such as metal ions like silver (Ag) or iron (Fe), can improve their photocatalytic ability and antibacterial activity. When compared to ZnO NPs, the ZnO-Ag NCs have better photocatalytic activity and photostability. Because nanoscale Ag^{2+} has antimicrobial properties, it would be a fascinating and beneficial addition to ZnO NPs, as it not only improves the particles' photocatalytic activity but also their antibacterial properties (Arooj *et al*., 2015).

2.5 Properties of ZnO nanomaterials

Semiconductors with nanometer-scale dimensions are important because their electrical, optical, and chemical properties can be tuned by altering particle size.

2.5.1 Electrical properties

Fundamental research into the electrical properties of ZnO NPs is critical for future nanoelectronics applications. At room temperature, ZnO has a moderately large bandgap of 3.3 eV. Higher breakdown voltages, the ability to sustain large electric fields, high-temperature, and high-power operations are all advantages of a large bandgap. In the absence of doping, ZnO has an n-type character. A non-stoichiometry analysis is usually the source of the n-type character. Zinc interstitials and ZnO nanowires are said to exhibit n-type semiconductor behavior due to imperfections such as oxygen vacancies. The wide range of applications in electronics and photonics, combined with the complexity of p-type doping, is ZnO's biggest drawback. The benefits of p-type doping for ZnO nanostructures will greatly improve their future advanced applications in nanoscale electronics and optoelectronics. ZnO nanowires, both p-type and n-type, can be used as p-n junction diodes and light-emitting diodes (LED) (Fan & Lu, 2005).

2.5.2 Optical properties

The optical emission and nonlinear optical characteristics of nanomaterials with tiny particle sizes are increased. Due to quantum confinement phenomena, nanoparticles formed of semiconductor materials absorb and emit light at certain wavelengths that are heavily dependent on particle size and shape (Sali *et al*., 2021). ZnO is transparent to visible light but absorbs ultra violet light at wavelengths below 365.5 nm. White pigments absorb more light than other white pigments. Regular zinc oxide appears white in visible wavelengths, but rutile and anatase titanium dioxide have a higher reactive index and thus superior opacity. ZnO is a semiconductor with a large exciton binding energy of 60 meV and a wide band gap of 3.37eV (M. Zare et al., 2018). It is also one of the most promising semiconductor materials for electronic, photonic, optical, and biological applications. The energy of 3655 photons corresponds to the band gap energy that occurs between the valences and conducting bands. Under the analytical study of ultra violet light, zinc oxide is considered to be photoconductive (Ramani *et al*., 2012).

The combination of optical and semiconductor properties results in a doped ZnO that is a contender for new device generations. Solar cells necessitate intrinsic optical properties of ZnO nanostructures, which are currently being studied in depth for use in photonic devices. ZnO nanostructures' photoluminescence (PL) spectra have been extensively studied. The photoluminescence spectra of ZnO nanorods were used to investigate excitonic emissions. Quantum size confinement has been shown to increase the exciton binding energy significantly. There is a strong emission peak at 380 nm due to a band-to-band transition, as well as a green-yellow emission band due to oxygen vacancy. Photoluminescence spectra demonstrate that the ZnO nanowire is a capable and promising UV emitting material. Its UV lasing capability is also more significant and intriguing. ZnO nanowire or nanorod is a natural candidate for the optical waveguide due to its near-cylindrical geometry and large refractive index of nearly 2.0 (Kulkarni, 2015).

The excitonic recombination lowers the lasing threshold, and quantum confinement yields a substantial density of the band edges and improves radiative efficiency, which are both advantages of ZnO nanowire lasers. The use of dielectric nanowires to guide optical waves has also made significant progress. ZnO nanowires have recently been described as a sub-wavelength optical wave-guide. ZnO nanowire guided optically forced light emission and was coupled into SnO2 nanoribbon. These findings suggest that Optical properties are of great interest in optoelectronics, photovoltaics, and biological sensing applications. ZnO nanostructures could be useful components in integrated optoelectronic circuits. Optical properties have a great interest in the vast application of optoelectronics, photovoltaics, and biological sensing (Aneesh *et al*., 2007).

2.5.3 Chemical properties

ZnO is found in the form of zincite, a mineral, and zinc white, a white powder. Manganese impurity causes it to be orange or red. Thermochromic ZnO is crystalline zinc oxide that changes color from white to yellow when heated and then returns to white when cooled. At high temperatures, a very small loss of oxygen causes this color change. ZnO is amphoteric, meaning it reacts with acids as well as to alkalis. Zinc sulfate is formed when ZnO reacts with acid. It forms zincates when it reacts with alkali in the same way. ZnO decomposes into zinc vapor and oxygen, demonstrating its high stability. When ZnO is exposed to air, it absorbs both water vapor and carbon dioxide, forming zinc carbonate (Yu *et al*., 2011).

2.6 Application of Nanomaterials

2.6.1 Biomedical Applications

Metal oxide nanoparticles have a distinctive structure, a large surface area, are biocompatible, have fascinating redox and catalytic capabilities, and are mechanically stable. Because of these features and unique plasmonic properties, they are receiving a lot of attention in the area of biomedical applications as bioimaging, biomedical therapies, biosensing, implant devices, neurochemical monitoring and diagnostics, and so on (Annu *et al*., 2018). Nanomaterials such as ZnO, Fe_2O_3, Au, and Ag demonstrate good biocompatibility and nontoxicity and are now being studied extensively. ZnO has strong antibacterial activity making it ideal for external applications like wound dressing and coating for medical devices to avoid biofilm formation. Fe_2O_3 NPs MRI contrast agents, bioseparation and targeted administration, and tumor heat therapy. The longitudinal relaxivity of Au NPs is high, and they have luminous characteristics. Fluorescent Silica NPs are also employed in bioimaging because of their optical clarity, high hydrophilicity, and biocompatibility. Fe_2O_3 NPs retain their magnetic properties and have been discovered to be useful in a variety of sophisticated biomedical procedures, including magnetic resonance imaging contrast agents, bioseparation and targeted delivery, and hyperthermia therapy of tumors. Au NPs have a high longitudinal relaxivity value and exhibits fluorescent properties. Because of their biocompatibility, high hydrophilicity, optical transparency, and fluorescent Silica NPs are also utilized in bioimaging (Forruque *et al*., 2021).

2.6.2 Drug delivery

Because of their unique features, nanoparticles are rapidly being exploited in medicinal applications such as drug delivery, gene delivery, and cancer therapy. The utilization of nanoparticles in drug delivery and production has several benefits. Nanoparticles are used in drug delivery after being targeted to a specific area because they are simple to make (Forruque *et al*., 2021).

The wide range of qualities and properties of nanoparticles including optical and physicochemical properties, biocompatibility, viable flexibility, controlled dispersity, and nontoxicity, make them an attractive nano-carrier in drug delivery systems. The broad features of nanoparticles such as biocompatibility, optical, viable flexibility, physicochemical properties, nontoxicity, and controlled dispersity make them compelling nano-carrier in drug delivery systems. Other benefits

of utilizing nanoparticles include better protection for encapsulated drugs, better control over drug delivery, extending the clearance period for drug retention at the active site, increasing bioavailability and therapeutic efficiency, and decreasing fed/fasted variability, which improves drug stability (Gour & Jain, 2019).

The use of nanomaterials in the pharmaceutical industry has also proven to be fruitful. Nanoparticles have been used to control dosage for drug delivery to specific targets. This can significantly reduce drug side effects and overdosing. Patients' costs and pain will be reduced by reducing the number of drugs they take. One NP that has demonstrated its worth promise in this application is ZnO (Forruque *et al*., 2021).

2.6.3 Antimicrobial and antiviral effects

Nanoparticles have received growing attention toward effective antimicrobial applications due to the increasing incompetence of traditional antibiotics and antibiotic-resistant strains of bacteria. The bactericidal effects of nanoparticles are thought to be the result of a combination of their size and high surface-to-volume ratio, which allows them to interact strongly with the bacterial membrane, rather than only due to the release of metal ions (Ali & Ahmed, 2018).

Various studies have been carried out to improve antimicrobial functions because of the growing microbial resistance to common antiseptics and antibiotics, according to Singh *et al*. (2018). According to in vitro antibacterial investigations, the metallic nanoparticles efficiently inhibit numerous microbial species. Metallic nanoparticles' antibacterial activity is determined by two factors: (a) the substance utilized to manufacture them and (b) their particle size. Smaller nanoparticles have a stronger antibacterial activity, allowing for more surface exposure to the bacterial membrane (Tang *et al*., 2013). Furthermore, these nanoparticles penetrate cell membranes more easily, interacting with intracellular materials and ultimately causing cell destruction during the multiplication process (Rezaei-zarchi *et al*., 2010).

The antibacterial activity could be explained using reactive oxygen species (ROS) such as hydrogen peroxide (H_2O_2), hydroxyl radicals (OH-), and singlet oxygen (O-), as evidenced by the fact that nanoparticles cause oxidative stress in bacteria and induce ROS. Microorganisms are thought to have a negative charge, whereas metal oxides have a positive charge. The microbe and the treated surface form an electromagnetic attraction as a consequence of this (Henderson, 2006).

Metal oxides like ZnO, CuO, Fe_2O_3, TiO_2, MgO, CeO_2, CdO, and CoO nanoparticles are also reported to exhibit high activity against different varieties of bacteria (Ali & Ahmed, 2018). According to the study by Forruque *et al*. (2021), ZnO NPs, which have a photocatalytic and photo-oxidizing effect, are known for their antifungal and antibacterial properties. The particle is also thought to be biosafe. ZnO NPs are effective against microorganisms with sizes ranging from nanometers to micrometers. Because of its size, the particle works best by entering the bacterial cell and disrupting the internal mechanisms (nano-scaled). Its antibacterial properties are aided by its high volume to surface area ratio and unique physicochemical characteristics. ZnO NPs and ZnO-Ag NCs acquired through green synthesis are also valuable in clinical antimicrobial wound-healing bandages (Gour & Jain, 2019).

2.6.4 Textile industry

Nanoparticles are becoming popular for coating and finishing textile fabrics in order to exploit their antimicrobial properties to decrease odor-producing bacteria and fungi and to reduce bacterial contamination that may cause disease (Yang *et al*., 2021). Microbes can cause damage to textile fabrics. To avoid this, the textile industry has been developing antimicrobial textile products. Nanoparticles, on the contrary, can be harmful. As a result, biosynthesized nanoparticles are now being used to create microbe-resistant textiles. ZnO, TiO_2, SiO_2, and Ag NPs are among the metal nanoparticles applied in different textile fabrics because they have strong antibacterial properties and unique characteristics such as UV absorption and self-cleaning (Forruque *et al*., 2021).

2.6.5 Wastewater treatment

Contamination of water sources is one of the major concerns in recent years. The treatment of wastewater is one way to address this raging problem. Traditional methods, however, due to time constraints and the occurrence of toxic contaminants, are unable to completely remove pollutants from water. Nanoparticles have the potential to help clean up polluted water (Forruque *et al*., 2021). Nanoparticles such as ferric oxide (Fe_3O_4), graphene, titanium oxide (TiO_2), magnesium oxide (MgO), manganese oxide (MnO_2), and zinc oxide (ZnO) are effectively used as adsorbents for the removal of contaminants such as heavy metals, azo dyes, etc. from water (Gupta & Kim, 2021).

2.6.6 Food industry

NPs in combination with other technologies can bring impactful innovations in the production, storage, packaging, and transportation of food products. The application of nanotechnology in the food industry is based on nanostructures that target food ingredients as well as sensors. Nano-food components cover a large area of applications starting from the processing of food to its packaging. In food processing, nanoparticles are used as antimicrobials, nano additives, nanocarriers, anticaking agents, and nanocomposites, while in food packaging, they are used as nano-sensors to check the quality of the food produced (Gupta & Kim, 2021).

Zinc supplements contain ZnO nanomaterials. Because of their antimicrobial properties, ZnO NPs are also used in food packaging. This aids in the prevention of food contamination caused by bacteria. ZnO NPs can also absorb UV light, which can protect UV-sensitive foods (Forruque *et al*., 2021).

2.6.7 Photocatalytic Applications

Another important and overwhelming area of research is the catalytic activity of MONPs. As a result, there were numerous reports on the catalytic activity of biosynthesized nanoparticles used to degrade hazardous dyes such as methyl red, methylene blue, crystal violet dye, safranine, and methyl orange, among others (Annu *et al*., 2018).

2.7 Bacterial Strains

2.7.1 Staphylococcus aureus

Staphylococci are gram-positive bacteria with individual cocci that appear to be divided into multiple planes, forming a grape-like cluster. They are facultative anaerobes that are neither motile nor spore-forming, and they grow through fermentation or aerobic respiration pathogenicity. *Staphylococci aureus* (*S. aureus*) is a member of the staphylococci genus, and it gets its name from the golden color it takes on when grown on solid media (Masalha *et al*., 2001).

2.7.2 Escherichia coli

Escherichia coli (*E.coli*) is a gram-negative bacteria that is both a natural part of human flora and a major pathogen that is a major cause of morbidity and mortality around the world. Both aerobic and anaerobic conditions make *E.coli* strains relatively easy to grow. Some *E.coli* isolates are thought to be part of the intestine's beneficial normal flora, but others appear to have acquired

pathogenicity mechanisms that cause diseases in humans, such as urinary tract infection, sepsis, or meningitis (Kaper *et al*., 2004).

2.8 Buddleja Polystachya

B.polystachya is a multi-branched small tree or shrub endemic to the semi-arid highlands surrounding the Red Sea in Saudi Arabia, Yemen, Somalia, Ethiopia, and Eritrea where it grows around a forest or in secondary scrub, most of the time alongside watercourses, at elevations ranging from 2,200 to 3,600 meters; its range extends southward into the highlands of Tanzania and Kenya (Leeuwenberg, 1979). Georg Fresenius was the first to name the species in the early 1800s.

B.polystachya typically grows to a height of 5 meters, but in the right conditions, it can reach a height of 12 meters. The bark can be reddish-brown or grey in appearance. The flowers are bright orange and form dense panicles up to 20cm long. The scent is described as being sweet to acrid. The leaves are up to 15 cm long and narrow, with a pointed tip, and a pale grey-green upper surface. A small dry orange capsule is the fruit (Chaudhary, 2001).

Buddleja species have piqued interest as anti-inflammatory, analgesic, antipyretic, antihepatotoxic, hypotensive, hypoglycemic, neuroprotective, antimicrobial, molluscicidal, and amebocidal remedies in traditional medicine (El-Domiaty *et al*., 2009). In Chinese traditional medicine, they've been used to treat cancer and to treat articular rheumatism (Hu et al., 2001). Various phytochemical compounds including triterpenoids, iridoids, flavonoids, and phenylethanoids have been isolated from *Buddleja* species in previous phytochemical studies (Tai *et al*., 2011). Furthermore, according to Kahsay (2017), phytochemical analysis of *B.polystachya* leaves reveals a high concentration of Flavonoids, Alkaloids, Terpenoids, Cardiac glycosides, oils, and Saponin compounds.

B.polystachya is known as ‘’Anfar’’ in Amharic in Ethiopia. *B.polystachya* is used by Ethiopians and people in other east African countries to treat a variety of skin conditions (Houghton, 1984). The microbicidal and cytotoxic activities of the various components obtained from *B.polystachya* have been reported (Fawzy *et al*., 2013). Furthermore, *B.polystachya's* crude extract had antidiarrheal and antispasmodic properties (Rehman *et al*., 2015). *B.polystachya* has previously

been used to isolate 16 compounds, including isobenzofuranone derivatives, phenolic fatty acid ester, flavonoids, and triterpenic acids (Al Ati *et al*., 2015).

2.9 Research Review and Gap

Nanotechnology is an innovative and emerging field that aims to create novel materials at the nanoscale. Nanomaterials, in contrast to their mass counterparts, are made up of small particles with a large specific surface area, resulting in materials with unusual surface area, volume, quantum size, and macro tunneling effects (Demissie *et al*., 2020). Nanomaterials exhibit unique optical, mechanical, catalytic, and biological properties because of these characteristics, resulting in nanomaterials having broad application potential (Kalpana & Rajeswari, 2018). As a type of nanomaterial, ZnO NPs are widely used in the fields of electrochemistry, medical devices, cosmetics, the textile industry, etc. because of their high specific surface area, biocompatibility, ultraviolet light absorption and scattering, and their antibacterial properties (Xu *et al*., 2021). There are many conventional physical and chemical methods that have been used for the synthesis of ZnO nanoparticles and ZnO –Ag NCs (Alavi & Nokhodchi, 2021). However, these approaches are usually costly, time-consuming, and possibly harmful to the environment and living organisms. The chemical method entails the use of toxic chemicals that can be detrimental to the environment as well as the person using them. Additional capping and stabilizing agents are required in both physical and chemical procedures. Organic solvents and reducing agents are used in the majority of these synthesis processes. (Agarwal *et al*., 2017) .

Thus, there is a clear need for a more cost-effective, safe, and ecologically friendly technique for producing nanoparticles. Therefore there is a need for "green synthesis" that offers numerous benefits of eco-friendliness, where toxic chemicals are not used for the synthesis process. In the green synthesis method plants, bacteria, fungi, algae, etc. are used. This method uses a biological approach in which different types of microorganisms/plant extracts are utilized to manufacture various metallic NPs. It has numerous advantages over other chemical approaches, including being greener, saving energy, and being more cost-effective (Ying *et al*., 2022). Several researchers investigated the biosynthesis of ZnO NPs and composites using plants and their parts, which has emerged as a viable alternative to chemical synthetic procedures because it does not necessitate complicated processes and provides natural capping agents.(Dinah *et al*., 2019 ; Gurgur *et al*., 2020 ; Dumbrava *et al*., 2019).

Upadhyay *et al*. (2020) synthesized and compared ZnO NPs using leaves extract of *Ocimum tenuiflorum* and chemical method using thiourea as capping agent and the results revealed that the nanoparticles synthesized by the green approach had small crystallite size and higher absorbance intensity. Despite the good properties, there were problems during synthesizing the ZnO NPs by green synthesis such as stability and aggregation, control of crystal growth, morphologies, sizes, and distribution, which are important issues that need further work to be solved. Other research by Hameed *et al*. (2019) also used a green method for the preparation of ZnO NPs and ZnO-Ag NCs using plant extract of *silybum marianum* for diverse biomedical applications. The nanoscale zinc-based particles produced by this approach were characterized based on absorbance intensity, as well as the morphology, particle size, and antibacterial activity. The outcome showed that the nanoparticles had low absorbance intensity and low antibacterial activity. However, this study did not investigate the effect of different reaction parameters such as temperature, time, pH, reactant concentration, etc. that can play important role in controlling the property of the NPs materials, so that should be optimized for achieving specific characteristics product. Similarly, Zare *et al*. (2018) also used a novel green biomimetic approach for the synthesis of ZnO-Ag nanocomposite which was utilized for antimicrobial activity against food-borne pathogens. However, the study was mainly focused on the factors that affect antibacterial activity. It did not investigate the best synthesis conditions of the nanoparticle that can improve the property of the nanoparticle and thus its application.

3. MATERIALS AND METHODS

3.1 Materials

3.1.1 Chemicals and Reagents

The following chemicals and reagents were used during the study: silver nitrate ($AgNO_3$), zinc acetate dihydrate (Zn $(CH_3COO)_2.2H_2O$) (LOBA CHEMIE, 98%), sodium hydroxide (FINEM, 97%), sulfuric acid (UNICHEM, India, 98%), hydrochloric acid (35.4%), bromine water, chloroform (99.8%), ferric chloride, gentamycin, Muller-Hinton agar, nutrient broth, potassium bromide (solid), ethanol, and distilled water. All chemicals were analytical grade and used without further purification.

3.1.2 Apparatus and Equipment

The apparatus and instruments used for this research during the experiment session were beakers, measuring cylinder, conical flask, volumetric flasks, mortar and pestle, sieves, filter paper (Whatman no.1), analytical balance, hot plate and magnetic stirrer, oven, pH meter (model number pH−9202), oven dryer (model number DHG-9203A), air furnace (model number L31M), the ceramic crucible, centrifuge, test tubes, centrifuge, pipets, agar plates, spatulas, thermometer, and Erlenmeyer flask.

3.2 Raw Material Collection and Preparation of *B.polystachya* Leaf Extract

3.2.1 Plant raw material collection

The sample of *B.polystachya* was collected from Jimma Agricultural Research Center which is located at 7°40' latitude north and 36°50' longitude east and laid at an altitude of 1753 meters above sea level. The sample plant material was taken to the laboratory of the School of Chemical Engineering at Jimma University, Institute of technology.

The fresh leaves of *B.polystachya* were cleaned by washing several times with tap water and subsequently with distilled water to remove dust and debris. The leaves were then dried at room temperature in shade for about 10 days until all moisture become lost. Once the moisture of the leaves was removed in shade drying the dried leaves were ground using mortar and pestle which grinds the material into fine particles to increase the contact area of the leaves for maximum extraction. Thus, it was ground and sieved to about 5mm average particle size. The ground leaves

were stored in an air-tight container at room temperature for subsequent cycles of extract preparation.

3.2.2 Preparation of *B.polystachya* leaf extract

The leaf extract of *B.polystachya* was prepared according to the procedures by Demissie *et al*. (2020) with slight modifications. Thus, from the finely ground leave powder, about 10g of the leaves were mixed with 300 mL of distilled water in a 1000mL beaker and heated at 60 °C for 60 minutes until the color of the aqueous solution changed from light green to dark yellow. The resulting extract was cooled at room temperature and filtered by Whatman filter paper no.1. The percentage extract yield was calculated using equation 3.1 below:

$$\text{Percentage of extract yield} = \frac{W_e}{W_l} * 100 \qquad 3.1$$

Where

We is the weight of extracted dye (g), and

W_l is the weight of the leaf sample before extraction (g)

The extract was stored in a refrigerator at 4°C to be used for further experiments. The extraction procedure was repeated until enough amount of plant extract had been achieved. Figure 3.1 shows the dried leaves of *B.polystachya* and its extract.

(a)

(b)

Figure 3.1 *B.polystachya* (Anfar) leaf (a) and its extract (b)

3.2.3 Phytochemical screening of *B.polystachya* leaf extract: Qualitative analysis

The presence of different reducing, stabilizing, and capping agents in the leaf extract of *B.polystachya* was performed using standard methods of phytochemical screening according to (Karande *et al*., 2016) and (Gul *et al*., 2017) with some modifications. The qualitative phytochemical screening was performed to investigate the presence of common phytochemical constituents of plant extract such as tannins, steroids, saponins, phlobatannins, flavonoids, phenols, glycosides, and terpenoids.

(i). Test for tannin: 5 ml of bromine water was added to 1 ml of *B.polystachya* leaf extract. Decoloration of bromine water is an indicator of the presence of tannins in the plant extract.

(ii) Test for steroids: H_2SO_4 and chloroform each of 2 ml was added to 5 ml of the *B.polystachya* aqueous extract. The appearance of red color on the bottom layer of chloroform was an indication of steroids' presence in the plant extract.

(iii) Test for phlobatannins: 2 ml of 1% hydrochloric acid was mixed with 5 ml of the plant extract and then boiled using a hot plate stirrer at 25°C. The formation of red precipitate was an indication of the presence of phlobatannins in the plant extract.

(iv) Test for saponins: The presence of saponins in the *B.polystachya* leaf extract was checked by mixing 1 ml of the plant extract with 5 ml of distilled water and consequently shaken for 10 minutes. Thus, the formation of foam was evidence for the presence of saponins.

(v) Test for flavonoids: 3 ml of 10 % ferric chloride was added to 0.5 ml of the plant extract and shaken for 10 minutes. The formation of wooly brownish precipitate was an indicator of the presence of flavonoids in the plant extract.

(vi) Test for phenols: 5 ml of *B.polystachya* leaf extract was mixed with 2 ml of 2 % ferric chloride solution. The formation of blue-green or black color was evidence for the presence of phenol.

(vii) Test for glycosides: 2 ml of 5 % aqueous NaOH solution was added to 5 ml aqueous extract of *B.polystachya.* The appearance of reddish-brown color was evidence for the presence of glycosides in the plant extract.

(viii) Test for terpenoids: 2 ml of chloroform was mixed with 5 ml of *B.polystachya* leaf extract and evaporated at 60°C using a water bath. Consequently, 3 ml of sulphuric acid was added and boiled. The appearance of grey color was an assurance of the presence of terpenoids in the plant extract.

3.3 Preparation of ZnO Nanoparticles and ZnO-Ag Nanocomposites

3.3.1 Preparation of ZnO nanoparticles

The biosynthesis of ZnO NPs was conducted based on the modified procedures adopted from Oluyamo & Omotunde (2020). However, the formation of nanoparticles can be affected by different experimental parameters. Thus, considering their effect, the optimum synthesis values for ZnO NPs were taken from a previous study by Shabaani *et al*. (2020). Accordingly, 0.05M of precursor solution was prepared first using Zinc acetate dihydrate ($Zn(CHOO)_2 \bullet 2H_2O$) mixing with distilled water in 250 mL conical flask and it was heated at 25°C under magnetic stirring for about ten minutes. In a 5:1 ratio, 100 mL of the precursor solution was combined with *B.polystachya* aqueous extract in a dropwise step. Consequently, 10 mL of NaOH (1M) was added to the solution in a drop-by-drop fashion to bring the pH of the solution into the alkaline range (11.60). Under ambient circumstances, the finished mixture was agitated for an hour with a magnetic stirrer. The resultant solution was centrifuged three times at 3500 rpm with distilled water followed by ethanol to eliminate undesirable impurities after cooling to room temperature. The resulting precipitate was then collected and oven-dried at 105 ℃ for three hours. Finally, the powder was calcined using an air furnace for 2 hours at 400 ℃ to collect ZnO nanopowder. The calcination temperature was selected based on a previous study by Kennady & Madhu (2020) which reveals that a calcination temperature of 400°C is enough to synthesize highly crystalline ZnO nanostructures. After calcination, the ZnO powder sample was carefully placed in a clean sample holder for further characterizations of the nanoparticles. The diagrammatic representation of the synthesis of the ZnO NPs is illustrated in Figure 3.2.

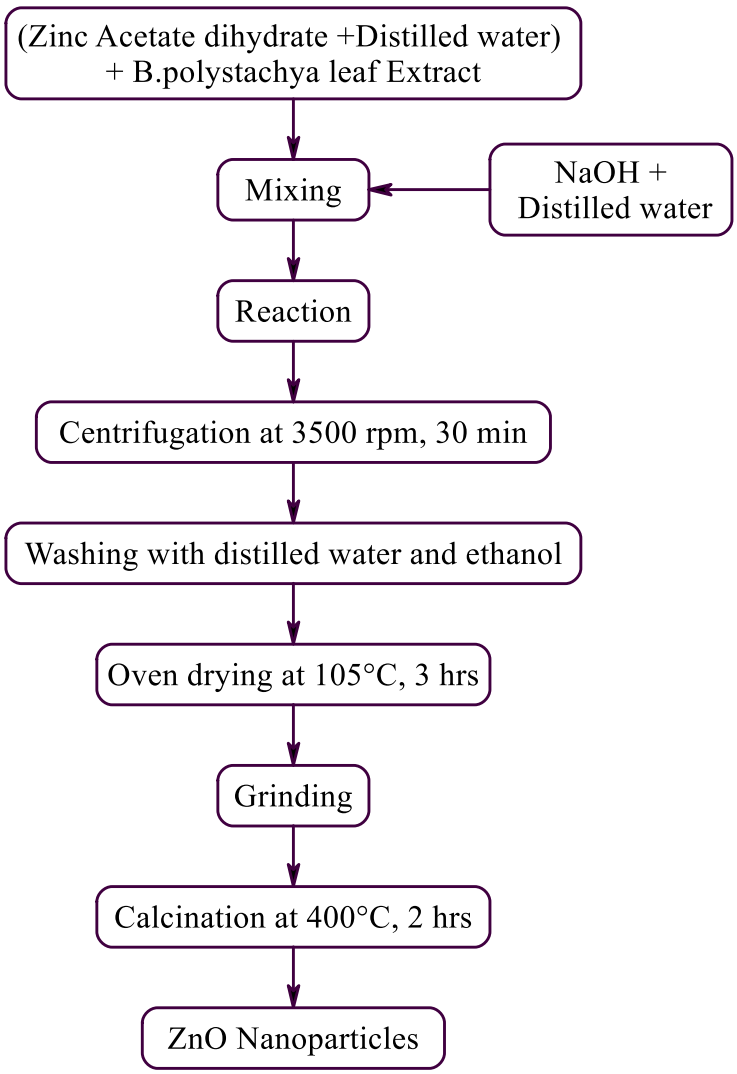

Figure 3.2 Synthesis of ZnO nanoparticles

3.3.2 Preparation of ZnO-Ag nanocomposites

ZnO-Ag NCs were synthesized according to the procedures adopted by Oluyamo & Omotunde (2020) with some modifications. Thus, solutions of Zinc acetate dihydrate (0.5M), Silver nitrate (0.05M, 0.075M, and 0.1M), and sodium hydroxide (1M) were prepared in separate conical flasks. The synthesis process was carried out at different levels of pH, the concentration of silver salt, and stirring temperature to study their individual and interaction effects on the product property. Thus, 100 mL (0.5M) of Zinc acetate dihydrate was mixed with 100 mL (0.05, 0.075, and 0.1M) $AgNO_3$ in separate 1000 mL conical flasks. The solution was stirred under the stirring condition for 5 minutes and 100 mL of the plant extract was added to each flask in a drop-wise process. NaOH solution was added to adjust the pH of the solutions to 7, 8.5, and 10. The solutions were stirred

with a magnetic stirrer for 1 hour at different temperatures (25, 40, and 55°C) and allowed to stand for 2 hours. The finishing process of ZnO-Ag NCs was similar to that of ZnO. Thus, the resulting solution was centrifuged three times at 3500 rpm with distilled water followed by ethanol to remove unwanted impurities after cooling to room temperature. The precipitate was then collected and oven-dried for three hours at 105°C. Finally, the powder was calcined for 2 hours at 400 °C in an air furnace to obtain ZnO-Ag nano powder. The ZnO-Ag powder sample was carefully placed in a clean sample holder after calcination to allow for further characterization and application. Figure 3.3 shows the diagrammatic representation of the synthesis of the ZnO-Ag NCs.

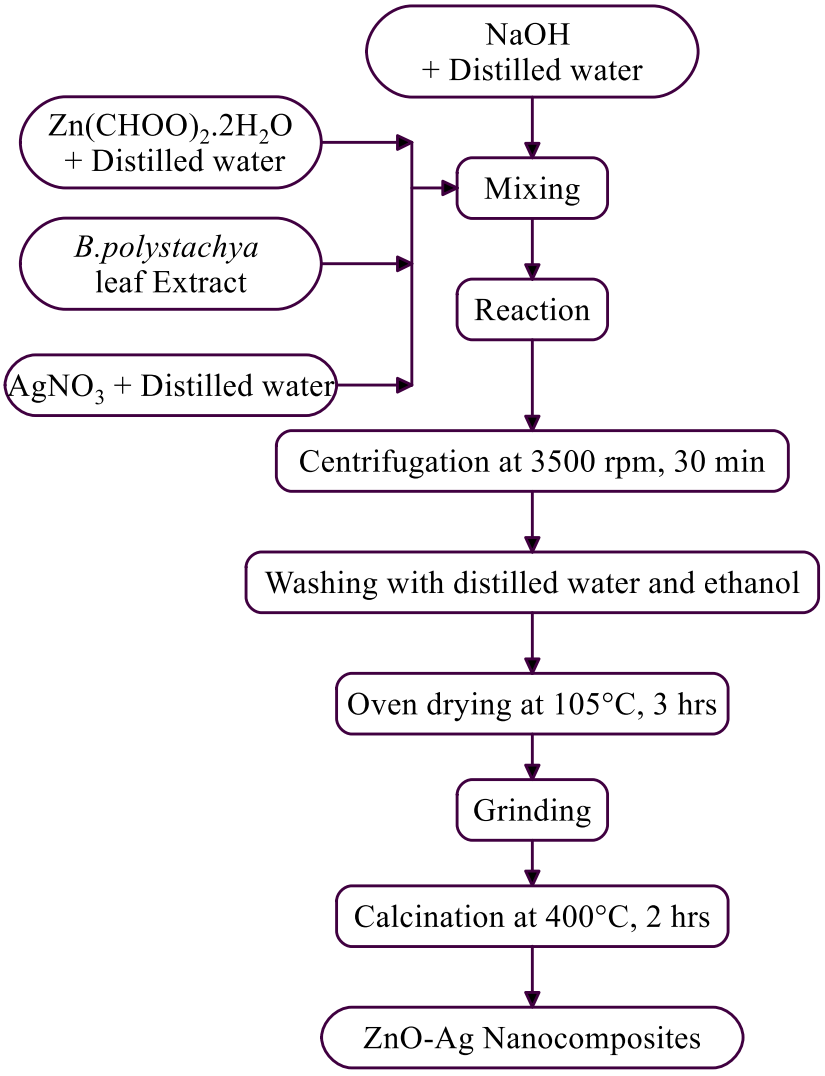

Figure 3.3 Synthesis of ZnO-Ag nanocomposite

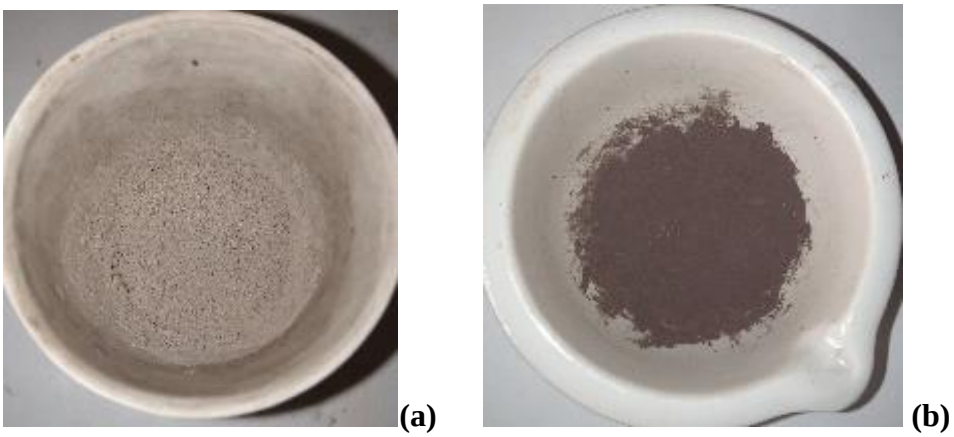

(a) **(b)**

Figure 3.4 biosynthesized ZnO NPs (a) and ZnO-Ag NCs (b)

3.4 Optimization of synthesis conditions using CCD

A central composite design (CCD) was used to obtain optimal synthesis conditions for the preparation of ZnO-Ag NCs. As a confirmation of nanoparticle production, this method was used to achieve the highest possible absorbance intensity. Temperature, pH, and the concentration of silver salt are the most important experimental operating parameters that may influence the absorbance of ZnO-Ag NCs. Data analysis was performed using design expert software (version 11.1.2.06, STAT-EASE Inc., Minneapolis, USA) to find the optimum conditions of the parameters for absorbance intensity of the NCs. The experiments were designed using the central composite design, which reduces the number of runs while also allowing for efficient estimation of the terms in the regression model. The goal of the experiment was to look into the single and interaction effects of a few optimum parameters. The results of the experiments were investigated using analysis of variance (ANOVA).

In most cases, green technology nanoparticle synthesis necessitates temperatures of less than 100°C or room temperature (Patra & Baek, 2014). In this study, the reaction temperature for the synthesis of ZnO-Ag NCs was selected as 25, 40, and 55°C. A report by Shah *et al*. (2015) states that bigger particles are formed at lower acidic pH levels than at higher pH values. When NPs are synthesized at a lower pH, particle agglomeration occurs, resulting in massive NPs and poor absorbance intensity. Particle nucleation, on the other hand, occurs when NPs are synthesized at a higher pH, resulting in small particles with a high absorbance intensity. Thus, in this study, a pH value of 7, 8.5, and 10 was selected for the synthesis of the NCs. Moreover, according to Bipin & Art, (2020), a reactant metal salt concentration in the range of 0.1–100 mM or even higher

concentrations are advisable for the synthesis of NPs. Therefore, 50, 75, and 100 mM concentration of Ag salt was selected for this study. Table 3.1 shows the summary of the empirical experimental operating parameters with their respective levels for the optimization of ZnO-Ag NCs synthesis.

The synthesis of ZnO-Ag NCs was fitted using a second-order polynomial equation and multiple regression of the data was carried out for obtaining an empirical model related to the most significant factors. The general form of the second-order polynomial equation (Wijaya *et al.*, 2019) is given in equation 3.2 below.

$$Y = \beta_o + \sum \beta_i x_i + \sum \beta_{ii} x_i^{\,2} + \sum \beta_{ij} x_i x_j \qquad 3.2$$

Where: Y is the predicted response, x_i and x_j are independent factors, β_0 is the model intercept, β_i is the linear coefficient, β_{ii} is the quadratic coefficient and β_{ij} is the interaction coefficient.

The following second-order polynomial model was used analogically to describe the relationship between the three independent variables and the response variable:

$$AI = a_0 + a_1A + a_2B + a_3C + a_{12}AB + a_{13}AC + a_{23}BC + a_{11}A^2 + a_{22}B^2 + a_{33}C^2 \qquad 3.3$$

Where AI is the Absorbance Intensity (predicted response), a_o is the intercept, [a_1, a_2, a_3] are the estimated linear effects, [a_{11}, a_{22}, a_{33}] are quadratic effects, and [a_{12}, a_{13}, a_{23}] are interaction effects of independent variables which are ‘‘A’’ (temperature), ‘‘B’’ (pH), and ‘‘C’’ (concentration Ag salt).

The total experimental runs were found 20 based on the general formula for experimental design for three factors with three levels which is given in equation 3.3 (Bayuo *et al*., 2020).

$$2^k + 2k + k_c \qquad 3.4$$

Where, k is the number of independent parameters and k_c is the number of center points

This meant that the modeling and optimization procedure required 20 experimental runs, including 8 factorial runs, 6 axial runs, and 6 center runs.

Table 3.1 Experimental factors for the biosynthesis of ZnO-Ag NCs and corresponding levels.

Independent Variable	Unit		Variable Levels			
		Star-low (-α)	Low (-1)	Center (0)	High (+1)	Star-high (+α)
Temperature	°C	15	25	40	55	66
pH		6	7	8.5	10	11
Conc. Ag Salt	Mm	33	50	75	100	117

3.5 Characterization of biosynthesized ZnO NPs and ZnO-Ag NCs

When materials' dimensions are reduced to the nanoscale, they exhibit unique properties that differ significantly from their bulk counterparts. Their electronic and optical properties, for example, can change, as can their chemical properties, as well as their mechanical and structural stabilities. These characteristics make nanoparticles appealing for unique sensing applications while also complicating their characterization processes. As a result, the challenge is to find the right characterization techniques with the best capabilities for studying the properties of nanomaterials produced by these methods.

Nanoparticle characterization is critical for gaining a better understanding of and control over nanoparticle synthesis and applications. Nanoparticle characterization can be accomplished using a variety of methods. UV–Visible Spectroscopy, powder X-ray diffraction (XRD), dynamic light scattering (DLS), and Fourier transform infrared spectroscopy (FTIR), was used as characterization techniques in this study.

3.5.1 UV–Visible spectroscopy

The maximum absorbance intensity of the biosynthesized ZnO NPs and ZnO-Ag NCs from the leaves of *B.polystachya* were measured using of ultraviolet and visible absorption spectroscopy in the range of 200-800 nm wavelength scan and scan speed of 50 nm/s. The experiment was done using SPECORD 200 PLUS - 223E1128F (Analytik Jena, Germany) instrument at the laboratory of Analytical Chemistry in Jimma University. The instrument determines the absorbance intensity of the nanomaterials by measuring the amount of light intensity that pass through the solution of the nanomaterials using equation 3.4 as follow:

$$A = \log_{10}\left(\frac{I_o}{I}\right) \quad 3.5$$

Where:

A= Absorbance Intensity (a.u.),

I_o = intensity of the incident light (cd),

I = intensity of the light after it passed through the sample (cd).

Using the results of the characterization technique, the bandgap energy of the biosynthesized ZnO NPs and ZnO-Ag NCs was also determined using Einstein's photon energy equation (López *et al*., 2010).

$$E_g = \frac{hc}{\lambda} \quad 3.6$$

Where:

E_g= energy band gap (eV),

h = planks constant (6.626×10^{-34} Js),

c = speed of light (3.0×10^{8}m/s),

λ = maximum wavelength of the biosynthesized NPs and NCs,

*Conversion $1eV=1.6\times10^{-19}$J.

3.5.2 X-ray Diffraction (XRD)

The crystalline structure of the biosynthesized ZnO NPs and ZnO-Ag NCs was investigated by X-ray diffraction using an X-ray diffractometer. The XRD analysis was carried out using the DW-XRD-Y7000 instrument with CuKα radiation (λ= 1.54060 A°) at Jimma Institute of Technology, Faculty of Materials Science and Engineering, Jimma. The sample was swept from 2θ=10° through to 80°. The average crystallite size of the biosynthesized nanoparticles and nanocomposites was estimated using Debye Scherer's equation (Xu *et al*., 2008) which is given in equation 3.7 below.

$$D = \frac{K\lambda}{\beta \cos\theta} \quad 3.7$$

$$\beta = \frac{\text{FWHM in } 2\theta \times \pi}{180^{o}} \quad 3.8$$

Where:

D = is the crystallite size (nm),

K= 0.94 is the Scherer's constant,

λ = 1.54 A° is the X-ray source wavelength,

β = is the full width at half maximum (FWHM) intensity of the peak position (rad)

θ = is the peak position (degree).

3.5.3 Fourier Transform Infrared (FTIR) Spectroscopy

The surface chemistry of green synthesized nanoparticles and nanocomposites can be studied using FTIR spectroscopy. FTIR helps to detect organic functional groups such as carbonyls, hydroxyls linked to the surface of nanoparticles, as well as other surface chemical residues (Vijayalakshmi & Rajendran, 2012). The FTIR measurement (model: PerkinElmer spectrum 2) of the samples was carried out at Jimma Institute of Technology, Faculty of Materials Science and Engineering, Jimma at a wave number range of 4000-400 $cm^{-1.}$ The analysis was done using KBr for the solid samples (powder form of ZnO NPs and ZnO-Ag NCs).

3.5.4 Dynamic Light Scattering (DLS)

Dynamic Light Scattering Analysis (DLS) is a well-known method used to characterize the average particle size and size distribution of the nanoparticles and nanocomposites. Thus, the average size and the size distribution of the biosynthesized ZnO NPs and ZnO-Ag NCs were determined using DLS at Addis Ababa Science and Technology University (Addis Ababa) by using the Zetasizer Nano instrument (ZE3600).

3.6 Antibacterial Activity Test

3.6.1 Disc diffusion method

To investigate the herbal functionality of the nanomaterials, the antimicrobial properties of synthesized ZnO NPs and ZnO-Ag NCs were tested. The disc diffusion method was used to determine antimicrobial activity using a suspension of bacteria spread on nutrient agar (Igwe, 2018). Gram-negative *E.coli* and Gram-positive *S.aureus* bacteria were used for the antibacterial test. As a standard agent, dimethyl sulfoxide (DMSO) and gentamicin was used for negative and positive control respectively against both gram-positive and gram-negative bacteria. The antibacterial tests were conducted at the laboratory of Microbiology in Jimma University.

The antibacterial test was started by placing a nutrient broth of 5 mg dissolved in 100 ml distilled water in two agar plates. Microbial cultures (*S.aureus* and *E.coli*) were swabbed on the plates containing nutrient agar media. For even mixing, these bacterial cultures inoculated in nutrient broth were shaken for 24 hours at 100 rpm on a rotary shaker.

Solutions of ZnO NPs and ZnO-Ag NCs each with 500mg/ml were separately prepared. The antibiotic disc, ZnO NPs sample, and ZnO-Ag NCs sample were all divided into three sections on the two agar plates. Using a dispenser that dispenses multiple discs at the correct distance apart without unacceptable overlapping of zones, gentamicin, DMSO, ZnO NPs, and ZnO-Ag NCs were placed on the surface of each agar plate. The test was done in triplicate. The plates were inoculated and incubated for 24 hours at 37°C. The antimicrobial activity was then measured against the test bacteria (*S.aureus* and *E.coli*) to determine the zone of inhibition. Using a ruler and calipers, the diameters of zones of inhibition of the control and test strains were measured (Igwe, 2018). The percent activity index of the nanomaterials was calculated by using the following equation (Khan *et al*., 2020):

$$\text{Percent Activity Index (\%)} = \frac{\text{Zone of Inhibition (Tested)}}{\text{Zone of Inhibition (Standard)}} \times 100 \qquad 3.9$$

3.6.2 Determination of minimum inhibitory concentration (MIC)

Based on the minimum effective concentration determined from the agar disc diffusion assay, the minimum inhibitory concentration of the biosynthesized zinc nanomaterials was calculated by serial dilution method (Khan *et al*., 2020). MIC is the minimum concentration of the material

required to inhibit the growth of an organism. Distilled water was used for serial dilution containing a different concentration of ZnO NPs and ZnO-Ag NCs in suspension form. Thus, for the minimum inhibitory concentration measurements, the minimum effective stock solution (500 mg/ml) was serially diluted to give the concentrations of 250 mg/ml, 125 mg/ml, 62.5 mg/ml, and 31.25 mg/ml.

4. RESULTS AND DISCUSSION

4.1 Phytochemical Screening Analysis

In this study, the highest yield obtained from *B.polystachya* leaf extract was of 20.4% (w/w), which is close with the results in literature. Previous study by Getahun *et al*. (2021) revealed that the percentage yield for the crude extract of *B.polystachya* was 22.7% w/w. Other study by Atsbeha *et al*. (2017) also found about 22.16% yield of *B.polystachya* leaf extract.

Because of the existence of several key bio-components such as terpenoids, alkaloids, phenols, tannins, proteins, amino acids, polysaccharides, enzymes, vitamins, and saponins, plant extract is commonly employed as a potential substitute for the stabilizing and reducing agent (Ahmad & Kalra, 2020). The results of a phytochemical screening examination of isolated leaf extract of *B.polystachya* are shown in in Figure 4.1 and presented in Table 4.1. The principal chemical elements of the extracts derived from *B.polystachya* leaf extracts are tannins, steroids, phlobatanins, saponins, flavonoids, phenols, and terpenoids, as shown in Table 4.1. Previous study by Kahsay (2017) reveals that *B.polystachya* leaves had high concentration of terpenoids, phenols, flavonoids and saponin compounds.

Quite apart from their biological and therapeutic properties, metabolites have been shown to have excellent reducing and stabilizing abilities in the reduction of bulk metals to nano forms (Gurgur *et al*., 2020). As a result, the bioactive molecules presented in Table 4.1 are believed to reduce $Zn(CH_3COO)_2{\cdot}2H_2O$ and $AgNO_3$ and cap the biosynthesized zinc based nanomaterials afterward to control growth and avoid agglomeration of the nanoparticles. There are numerous reports in the literature that indicate that phenols and flavonoids play a role in the bio-reduction, synthesis, and stability of metal and metal oxide NPs. The presence of large OH groups in phenol and flavonoids is what causes zinc acetate dihydrate to be reduced to ZnO NPs. The C=O, C=O–C, and C=C groups of heterocyclic compounds have previously been reported to behave as stabilizers (Ahmad & Kalra, 2020). As Vanaja & Annadurai, (2013) reveals, the presence of phenols and terpenoids allows the plant extract to self-assemble and cap the metal nanoparticles formed, resulting in controlled morphology. Additionally, they are involved in successfully catalyzing and stabilizing the reduction of bulk material to nano ions (Gurgur *et al*., 2020). Due to the presence of the phytochemical constituents, the plant extract of *B.polystachya* had the expected strength to reduce and stabilize bulk materials of the host and dopant precursors and their resulting metal ions. The

absence of glycosides confirmed reports in the literature that it can only exist in plant storage tissues (Selim *et al*., 2008).

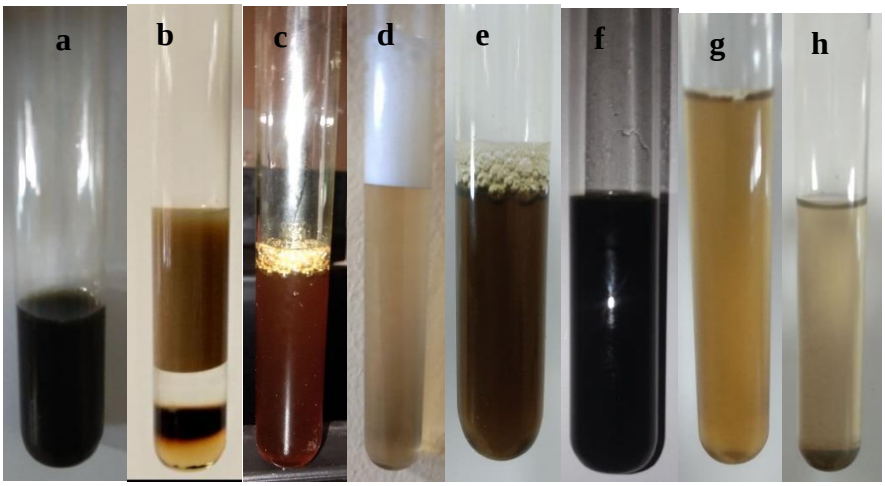

Figure 4.1 Phytochemical analysis of *B.polystachya* leaf extract: Tannins (a), Steroids (b), Phlobatainins (c), Saponins (d), Flavonoids (e), Phenols (f), Glycosides (g), and Terpenoids (h)

Table 4.1 Phytochemical constituents of *B.polystachya*

S.No	Phytochemical test	Observed color	Result
1	Tannins	Decoloration of bromine water	Positive
2	Steroids	Red	Positive
3	Phlobatainins	Red precipitate	Positive
4	Saponins	Formation of foam	Positive
5	Flavonoids	Wooly brownish	Positive
6	Phenols	Greenish black	Positive
7	Glycosides	Reddish brown	Negative
8	Terpenoids	Grey	Positive

4.2 Experimental Design and Statistical Analysis of Absorbance Intensity

4.2.1 Experimental design

The CCD approach was used in this study to determine the best experimental conditions for the green synthesis of ZnO-Ag NCs.

Table 4.2 Details of design runs for ZnO-Ag NCs synthesis and corresponding response (absorbance Intensity).

Std	Run	Factor 1 A: Temperature (°C)	Factor 2 B: pH	Factor 3 C: Ag Salt Concentration (mM)	Response 1 Absorbance Intensity
14	1	40	8.5	117	1.6282
1	2	25	7	50	0.6236
13	3	40	8.5	33	0.6069
18	4	40	8.5	75	1.6348
7	5	25	10	100	1.423
19	6	40	8.5	75	1.5933
4	7	55	10	50	1.0842
3	8	25	10	50	0.845
16	9	40	8.5	75	1.652
10	10	65	8.5	75	1.745
6	11	55	7	100	1.758
15	12	40	8.5	75	1.623
20	13	40	8.5	75	1.6321
11	14	40	6	75	1.105
2	15	55	7	50	0.9563
17	16	40	8.5	75	1.523
12	17	40	11	75	1.726
8	18	55	10	100	1.945
9	19	15	8.5	75	0.7547
5	20	25	7	100	0.845

CCD was employed to obtain the best absorbance intensity of the synthesized ZnO-Ag NCs while taking peak intensity into account. The objective was to explore three empirical synthesis factors: temperature (Temp), pH, and concentration of $AgNO_3$ solution.

Table 3.1 shows the three experimental factors used in the biosynthesis of ZnO-Ag NCs, as well as their corresponding five levels (3 levels and 2 boundary levels). Table 4.2 shows the experimental results of 20 runs created by CCD. Eight of the twenty experiments were factorial runs, which were included as cubic points, and six replication runs were suggested in level center points, which were used to clarify the pure error. Furthermore, six axial runs have been incorporated as star points for the proposed CCD. The six-star points were adjusted to a value of 0.2 to have a smooth design for experiments. Absorbance intensity was utilized as a response to the CCD design and modeling which resulted from recording the absorbance of 20 synthesized batches of ZnO-Ag NCs.

4.2.2 Statistical Analysis

The first step in conducting statistical analysis using a multivariate optimization method was to create a regression model with the absorbance intensity (target response) as the dependent variable and the experimental factors as the independent variables. Various linear and polynomial regression models were evaluated for this purpose, with different statistical parameters such as Fisher F-value using F-test (for both regression and lack of fit), squared correlation coefficient (R^2), adjusted R^2 (R^2 adj), and R^2 of prediction (R^2 pred) being used to select the best regression model.

4.2.2.1 ANOVA for absorbance intensity

Based on statistical parameters, a quadratic model was proposed to correlate the relationship among the experimental factors and the response (Absorbance Intensity). The ANOVA was constructed for this goal, which is represented in more detail in Table 4.3 because the goal of this part was to find conditions for obtaining maximum absorbance intensity.

Table 4.3 shows the performance parameters for the quadratic full model (FM), which includes all experimental variables (Temp, pH, and $Conc._{Ag}$), binary interactions (Temp × pH, Temp. × $Conc._{Ag}$, and pH × $Conc._{Ag}$) and self-interactions ($Temp^2$, pH^2, and $Conc._{Ag}^2$).

Table 4.3 ANOVA for Absorbance Intensity

Source	Sum of Squares	df	Mean Square	F-value	p-value	
Model	3.50	9	0.3886	87.57	< 0.0001	Significant
A-Temperature	0.9868	1	0.9868	222.39	< 0.0001	
B-pH	0.3408	1	0.3408	76.80	< 0.0001	
C-Ag salt Concentration	1.28	1	1.28	288.26	< 0.0001	
AB	0.0293	1	0.0293	6.61	0.0278	
AC	0.0931	1	0.0931	20.99	0.0010	
BC	0.0216	1	0.0216	4.87	0.0519	
A^2	0.2772	1	0.2772	62.47	< 0.0001	
B^2	0.0919	1	0.0919	20.72	0.0011	
C^2	0.4928	1	0.4928	111.07	< 0.0001	
Residual	0.0444	10	0.0044			
Lack of Fit	0.0335	5	0.0067	3.08	0.1214	not significant
Pure Error	0.0109	5	0.0022			
Cor Total	3.54	19				

The model F-value of 87.57 in Table 4.3 of ANOVA results indicates that the model is significant. In other words, it means that the regression equation could explain the majority of the variation in the response and that the model was significant. Furthermore, the $p<0.0001$ probability indicated that the model was significant. Due to noise, there is only a 0.01 percent chance that a Model F-value this large will occur. Model terms with P-values less than 0.0500 are significant. In this case, A, B, C, AB, AC, A^2, B^2, and C^2 are significant model terms. The model terms are not significant if the value is greater than 0.0500. As a result, linear terms of the parameters (Temp, pH, and Conc. $_{Ag}$) as well as linear interactions (Temp × pH and Temp × Conc. $_{Ag}$) and self-interactions ($Temp^2$, pH^2, and $Conc._{Ag}^2$) have a significant impact on absorbance intensity.

4.2.2.2 Model equation for absorbance intensity

According to the obtained results by RSM (Table 4.2), the range of the absorbance intensity was 0.6069–1.945. To fit the experimental data and based on a higher R^2 (0.9875) - and F values and a lower lack of fit, a quadratic model for the absorbance intensity of ZnO-Ag NCs was chosen which includes the main effect of variable, curvature effects, and the interaction between factors. The model equations that relate the response absorbance intensity of nanocomposite to the independent variables in terms of coded factors are shown in Equation 4.1 below.

Coded Equation**:**

$$\begin{aligned} Absorbance\ Intensity\ &= 1.61168 + 0.269808 * A + 0.158555 * B + 0.306174 * C - 0.0605625 * AB \\ &\quad + 0.107888 * AC - 0.140612 * A^2 - 0.0809783 * B^2 - 0.185103 * C^2 \end{aligned} \quad (4.1)$$

where A= Temperature

B= pH

C= Conc. Ag salt.

According to the ANOVA analysis, the interaction effect of pH and concentration of Ag salt (BC) in the absorbance intensity of ZnO-Ag NCs is insignificant. Thus, due to its insignificant effect BC was excluded from the final coded equation. All of the coefficients in the final codded equation are positive for all of the factors (Temp, pH, and Conc. Ag salt). The direct effect of temperature on the absorbance intensity may be due to an increase in the rate of nanoparticle formation (Tahir *et al*., 2015). As expected, increasing the pH has a positive effect on absorbance intensity, possibly due to increased ionization of active functional groups, particularly phenolic groups, in *B.polystachya* extract, which improves the extract's reduction ability and the production of ZnO-Ag NCs. Although the concentration of Ag salt has a direct relationship with absorbance intensity, it has the opposite effect on the size of ZnO-Ag NCs. Thus, the absorbance intensity of the NCs increases as the concentration of the Ag salt increases. It should be noted, however, that the proposed model is multi-parameter in nature, and the impact of other factors and interactions should be taken into account at the same time.

The coefficients sign determines the response performance. As can be seen in the coded equation, the coefficients of AB, A^2, B^2, and C^2 are negative, indicating decrease in absorbance intensity as the factors increase, whereas the coefficient of AC is positive, indicating that it has a positive effect on synthesis quality and, as a result, increase in absorbance intensity.

4.2.2.3 Model Statistics

Table 4.4 below shows that the variation coefficient (CV%) was found as 4.99 which is reasonably low and acceptable, indicating a better precision and reliability of the experiment. The model's correlation coefficient (R^2) and adjusted R^2 (R^2 adj) were calculated for further evaluation of the goodness of fit of the model. It had been suggested that the R^2 value should be at least 0.80 for a good fit of a model. As a result, the regression model was found to be highly significant, with values of R^2 and R^2 adj equal to 0.9875 and 0.9762, respectively, indicating a close agreement between the observed and the theoretical values predicted by the model equation (Figure 4.3) (Golbraikh & Tropsha, 2002). indicating a close agreement between the observed and the theoretical values predicted by the model equation R^2 adj is a better parameter than R^2 for a limited number of runs in models with a large number of variables because R^2 adj is adjusted to the number of variables and the size of runs (here 20) in the model. The R^2 pred was also 0.9189, indicating that the prediction ability was acceptable (Golbraikh & Tropsha, 2002).

Table 4.4 Model adequacy measures for absorbance Intensity

S.No	Response parameter	Absorbance Intensity
1	Std. Dev.	0.0666
2	Mean	1.34
3	C.V. %	4.99
4	R^2	0.9875
5	Adjusted R^2	0.9762
6	Predicted R^2	0.9189
7	Adeq Precision	31.1887

Adequate precision is a statistical indicator for model validation that can be used to estimate the signal-to-noise ratio. Our suggested model's adequate precision was 31.1887, which was significantly higher than 4 as the cut-off value for precision acceptance (Gheshlaghi *et al*., 2008).

As a result, the obtained model has been used for further process and optimization of ZnO-Ag NCs synthesis for the reasons stated.

4.2.2.4 Model diagnostics test

The normal probability of residual and also the internally studentized residual versus predicted response are two additional approaches that can be used to assess model accuracy. Figure 4.2(a) shows the normal probability plot of the residuals, which shows that all of the residual values lie along a straight line with no large deviations, confirming the normality of the distribution of the errors. Figure 4.2(b) also shows that the residuals are not only randomly distributed on both sides of the zero line (with no systematic pattern on one side), but also fall within the range of ±4σ. Furthermore, the adequacy of the model is shown from the predicted versus actual plots as shown in figure 4.3. The data points on the plot of the response were reasonably distributed around the straight line. This indicates a good relationship between the experimental and predicted values of the response. Moreover, it confirms that the underlying assumptions of the above analysis were appropriate. As a result, Figure 4.2 declares that the proposed quadratic model is acceptable, free of systematic error, and suitable for synthesis process optimization.

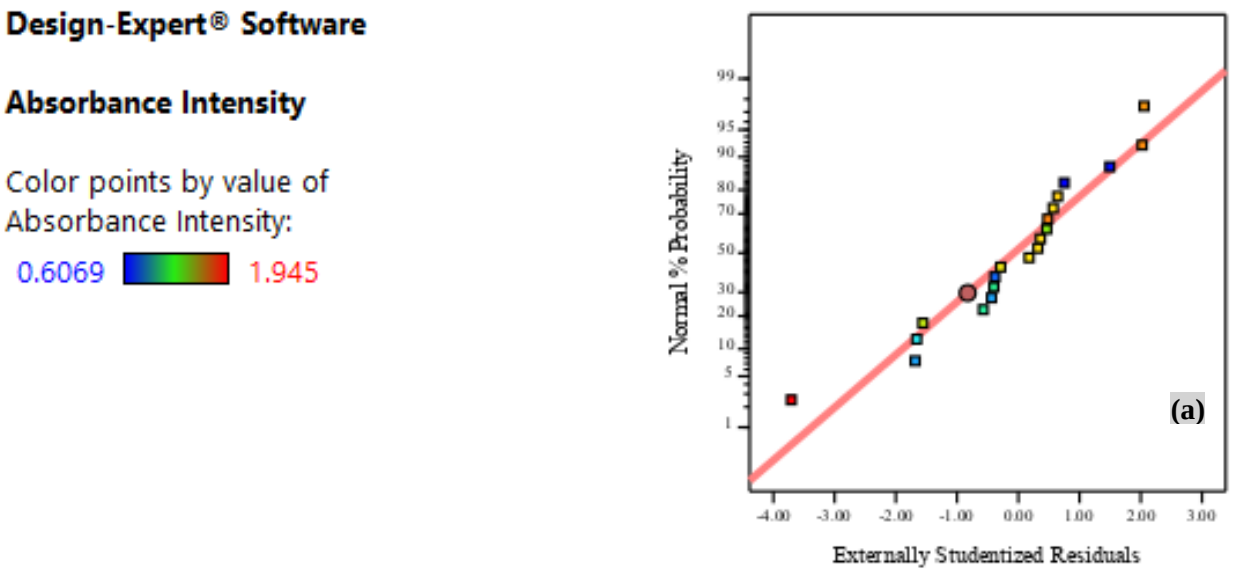

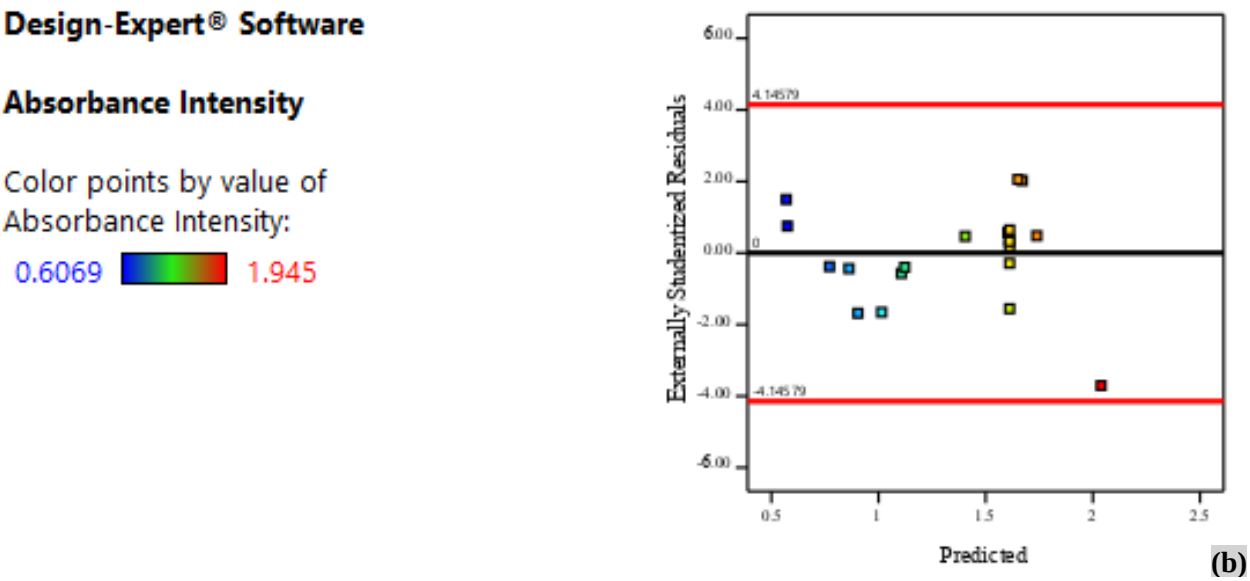

Figure 4.2 Plot of normal % probability versus internally studentized residuals **(a)**, studentized residual versus predicted **(b)**

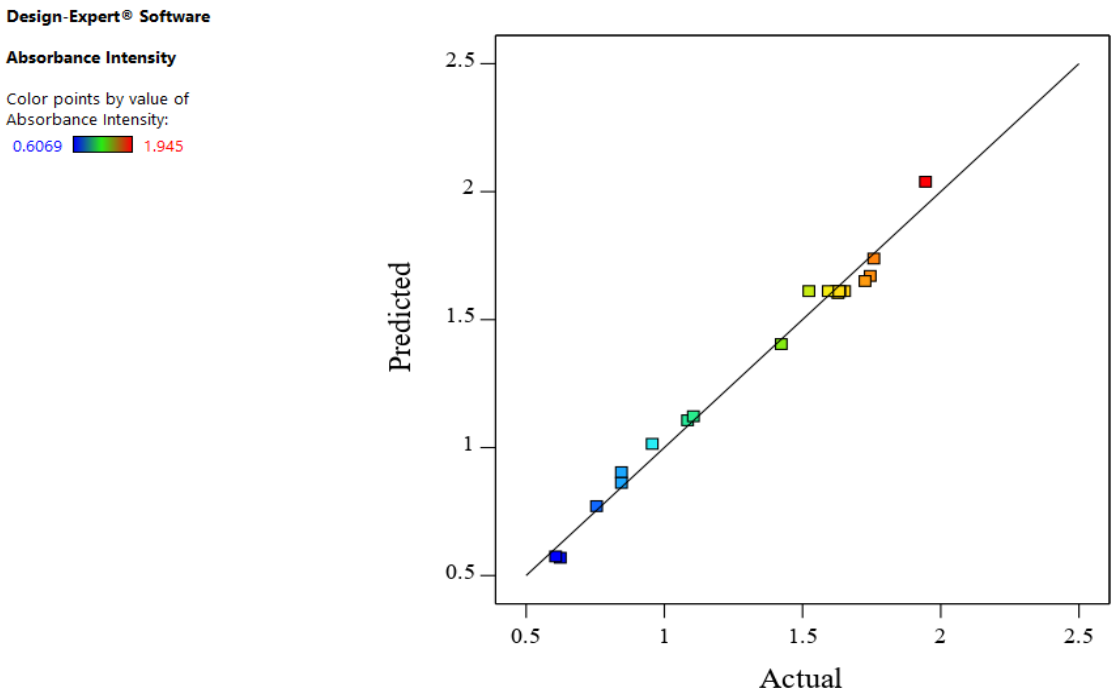

Figure 4.3 Plot of predicted versus actual absorbance intensity

4.2.3 Visualization and comparison of individual process variables and their interactions

4.2.3.1 Effect of individual process variables

Changes in parameters such as pH, temperature, and concentration, had a direct impact on the synthesis of ZnO-Ag NCs and increase or decrease in any of these parameters led to the improvement or cancelation of the process of synthesizing ZnO-Ag NCs. These parameters were studied to determine the best suitable condition for biosynthesis of ZnO-Ag NCs. After determining the optimal conditions in each of the effective parameters, the ZnO-Ag NCs were synthesized under optimum conditions and analyzed.

A. Effect of temperature

Temperature is important in green nanoparticle synthesis because it regulates the nucleation process during nanoparticle formation. At constant pH and Ag salt concentration in the center point, Figure 4.4 shows the temperature effect on the absorbance intensity of ZnO-Ag NCs. As observed, the absorbance intensity was increased significantly as the temperature rose from 25 to 53.7°C. The optimum temperature was found to be 53.7°C, as shown in the figure, since the ZnO-Ag NCs had the highest absorbance intensity. This may be owing to the formation of smaller particles at this temperature, which have more active sites due to their higher surface area, thereby increasing the absorbance intensity (Abdullah *et al*., 2020). On the other hand, the absorbance intensity of the nanocomposite remains constant after the temperature increases further beyond 53°C. This is due to the formation of bigger sized nanoparticles at higher temperatures. Zare *et al*. (2017) discovered that as the temperature rises, nanoparticles agglomerate. The collision frequency is increased at high temperatures due to faster reaction kinetics. As a result, atoms are more likely to collide and bind with one another, resulting in bigger particles. Furthermore, at low temperatures, the nucleation process is slow, allowing enough time for the nuclei to develop into a defined structure. The results of the ZnO-Ag NCs absorbance intensity as a function of temperature show that the solution's effective temperature is 53.7°C. As a result, the optimum temperature for the synthesis of ZnO-Ag NCs was chosen as 53.7°C. This is in agreement with the obtained model equation where the coefficient of temperature has a positive sign which indicates the increment of absorbance intensity as temperature increases.

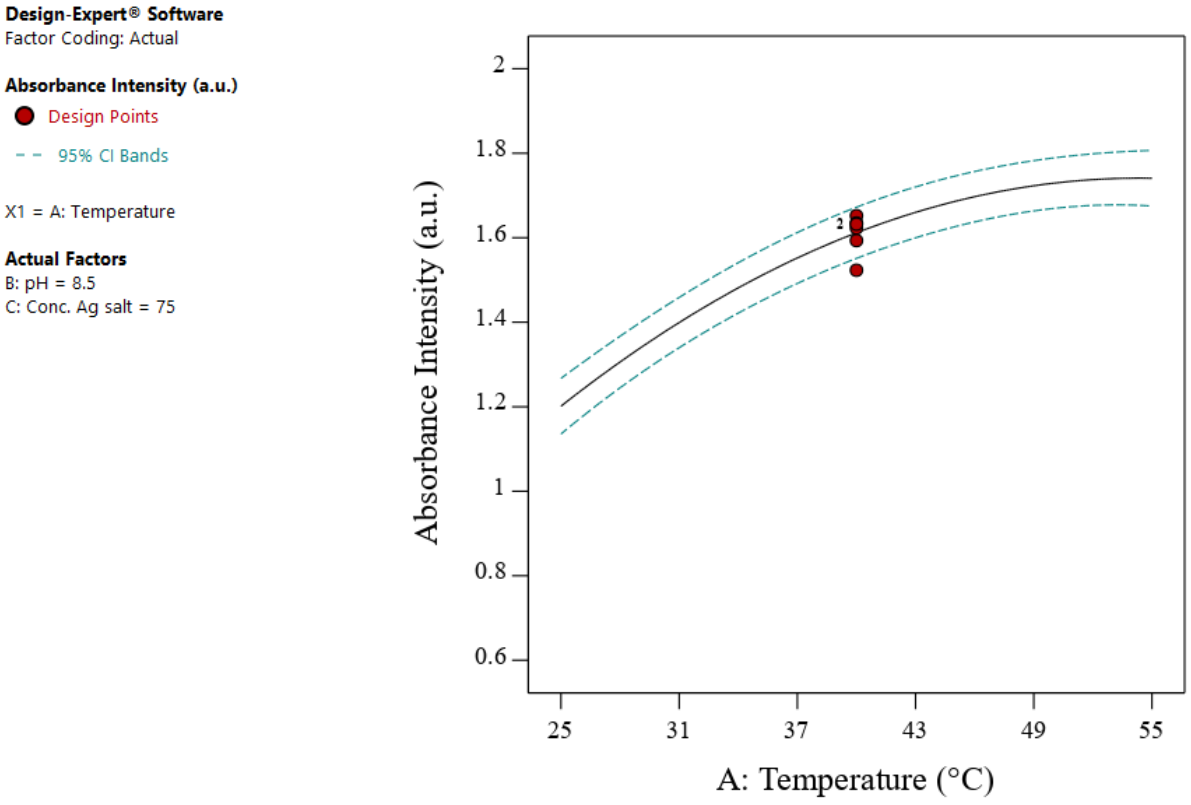

Figure 4.4 Temperature effect on Absorbance intensity of ZnO-Ag NCs

B. Effect of pH

The pH of a reaction mixture plays an important role in nanomaterial synthesis. The effect of pH on the absorbance intensity of ZnO-Ag NCs at constant temperature and Ag salt concentration in the center point is shown in Figure 4.5. As observed, the absorbance intensity of ZnO-Ag NCs was relatively low (i.e. 1.36) at pH value of 7. The absorbance intensity increased significantly from 1.35 to 1.612 as the pH increased from 7 to 8.8. The low absorbance intensity of the nanocomposites might be due to the formation of large size of nanocomposites resulting from aggregation of particles caused by low pH value of the reaction medium (Shah *et al*., 2015). However, as the pH value of the reaction mixture increases, particle nucleation occurs which results in the formation of small size nanocomposites that have high absorbance intensity. This may be due to the dissociated state for capping functional groups of the *B.polystachya* extract are influenced by the pH of the reaction solution. With the elevated pH, the deprotonation of the capping functional groups are strengthened. The deprotonated functional groups might carry more negative charge. Consequently, the negative charged groups bind to

the ZnO-Ag NCs and enhance the stability due to the electrostatic repulsion (Shabaani *et al*., 2020) .

On the other hand, there was a slight increment in absorbance intensity beyond pH = 8.8, which might be due to low rate of reduction of the zinc and silver ions at higher pH values. The absorbance intensity of the ZnO-Ag NCs as a function of pH revealed that the effective pH of the solution was 8.8, with no significant differences in absorbance intensity between pH 8.8 and pH 10. Thus, the result suggests that a more alkaline medium enhances the formation of ZnO-Ag nanocomposites. This is in agreement with the UV spectra that reveals the absorbance intensity of nanomaterials increases with increasing pH values. This might also be due to higher rate of reduction of zinc and silver ions at alkaline medium (Abdullah *et al*., 2020).

On the other hand, the coefficient of pH in the obtained model equation has a positive sign which implies the positive effect of pH on absorbance intensity of ZnO-Ag NCs. Thus, Figure 4.5 is in agreement with the obtained model equation.

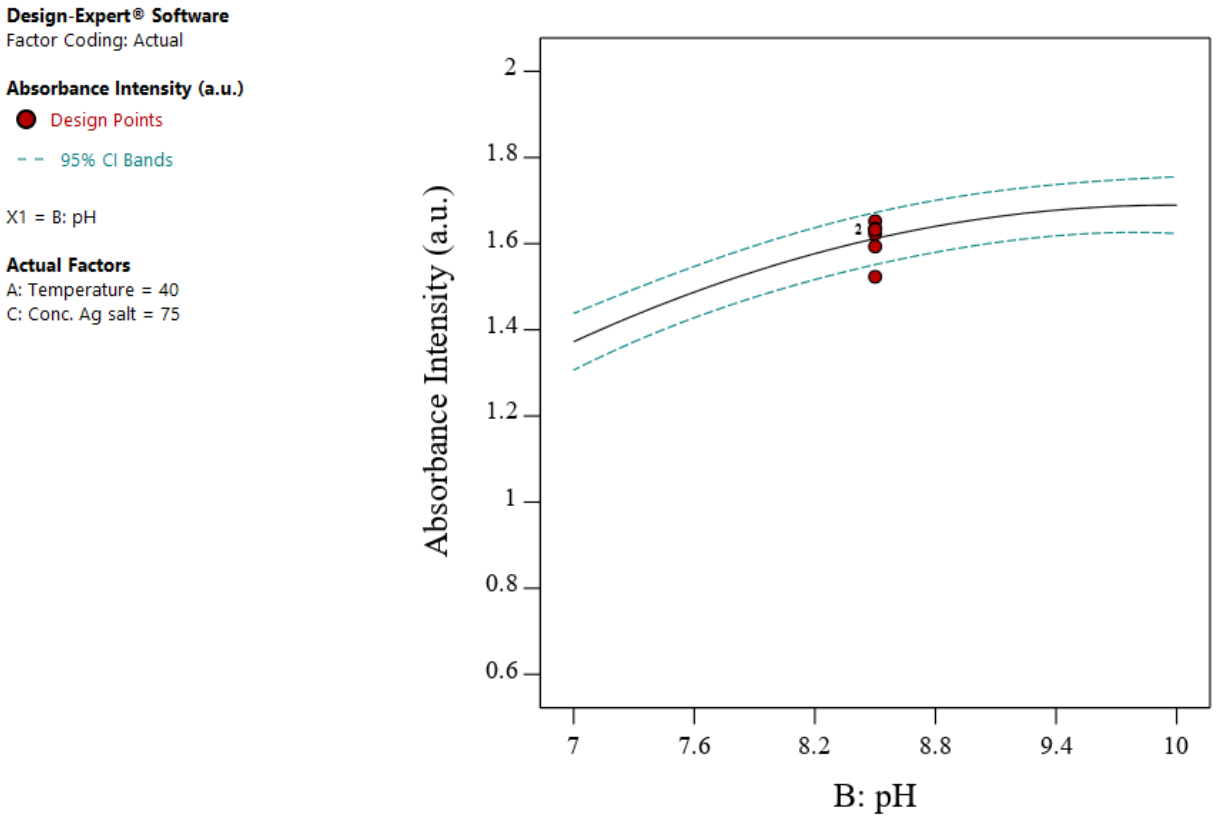

Figure 4.5 Effect of pH on Absorbance intensity of ZnO-Ag NCs

C. Effect of concentration of $AgNO_3$

The effect of Ag^{2+} dopant concentration was also investigated in the range of 50 to 100 mM. Figure 4.6 shows the effect of the concentration of Ag salt on the absorbance intensity of ZnO-Ag NCs at constant temperature and pH in the center point. The minimum absorbance intensity was obtained at 50 mM concentration of Ag salt which is 1.125 and it significantly increased to 1.948 as the concentration of Ag salt increased to 91.4mM. Thus, from figure 4.4 it is obvious to state that changes in absorbance intensity of ZnO-Ag NCs varied depending on the variations in the concentration of Ag salt. The optimum silver nitrate concentration for the maximum absorption intensity was discovered to be 91.4 mM. The absorbance intensity of ZnO-Ag NCs falls beyond this concentration. Because the reaction has achieved saturation, higher dopant concentrations result in reduced absorbance intensity. When the concentration of metal ions rises above a certain point, it prevents the dopant from shrinking in volume, reducing the number of particles created. Furthermore, raising the metal salt concentration results in greater particle size due to increased metal ion availability. Because of the strong attraction between the atoms, this causes agglomeration and aggregation of nanoparticles (Abdullah *et al*., 2020). As a result, the size of nanocomposites has a direct impact on the absorbance intensity, with smaller particles having a higher absorbance intensity than bigger ones. As a result, 91.4 mM was chosen as the concentration with the highest absorbance intensity. This is in agreement with the obtained model equation where the coefficient of concentration of Ag salt has a positive sign which is an implication of absorbance intensity increment as concentration of Ag salt increases.

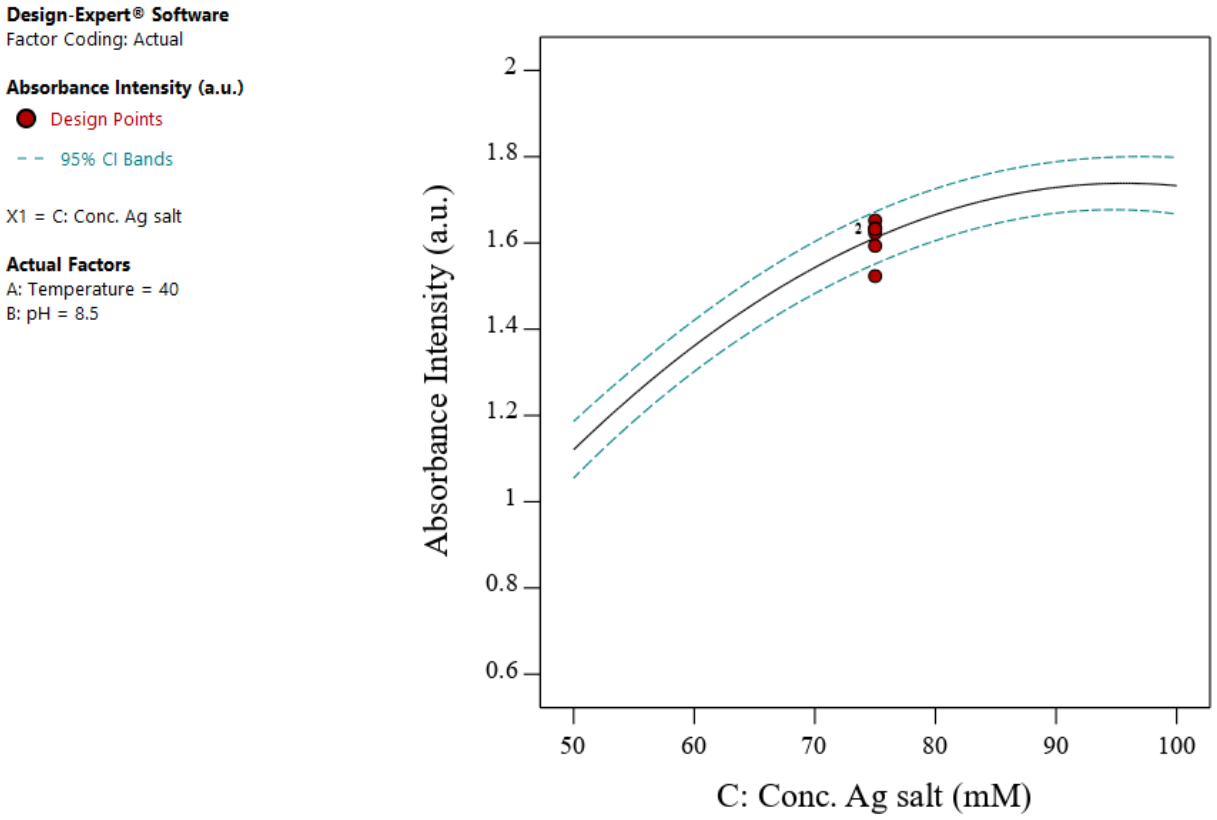

Figure 4.6 Effect of Volume of Ag salt on Absorbance intensity of ZnO-Ag NCs

4.2.3.2 Interaction effect of process variables on absorbance intensity

Figures 4.7 and 4.8 show contour plots and three-dimensional (3D) surface representations of various operational factors (independent variables) on the absorbance intensity of ZnO-Ag NCs (dependent variable) to investigate their effect. Contour plots, as seen in Figures 4.7(a) and 4.8(a), are a means to depict a three-dimensional surface on a two-dimensional plane. The 3D surface plot is a projection of the contour plot giving shape, in addition to the color and contour (Figure 4.7(b) and 4.8(b)). In this case, graphs were created by plotting the response surface (i.e. absorbance intensity) versus the two effective factors that show significant binary interactions, while other factors were kept constant at the applied CCD's central level.

As shown in Figure 4.7, the absorbance intensity was higher when concentration of Ag salt and temperature increased. It was observed that as temperature increased from 25 to 55°C and the concentration of Ag salt increased from 50 to 100 mM, the absorbance intensity of the nanocomposite was increased from 0.6 to 1.92, which means that it is in accordance with the

model. This might be explained that increasing metal ion concentration to a certain point allows growth of the nanocomposites at a faster rate and results in nanomaterials with smaller size and higher absorbance intensity. Besides, it was suggested that the increase in temperature decreases nanomaterials size and thus, increase absorbance intensity, which is normally due to increment in reaction rate and kinetic energy at elevated temperatures (Al-kordy *et al*., 2021). The combined result of the pH and concentration of Ag salt was also examined and the results are given in form of contours and 3D plots as shown in Figure 4.8. As can be seen, the absorbance intensity increased when concentration of Ag salt and pH was higher, revealing that positive interaction between them. As a result, the contour plot against absorbance intensity for pH and concentration of Ag salt showed that if the pH increases from 7 to 10 and the concentration of Ag salt increases from 50 to 100, the absorbance intensity of the nanocomposite increases up to 1.83. This may be due to the inactivation of biomolecules involved in the synthesis of ZnO-Ag NCs at low and high pHs (Al-kordy *et al*., 2021). Generally, pH plays a significant role in nanomaterial synthesis, mainly because it has the ability to alter the shape of biomolecules that is responsible in capping and stabilizing the NPs and NCs. The obtained data reveal that alkaline pH and a high metal concentration are conditions that will result in highest absorbance intensity of ZnO-Ag NCs. While, a higher or lower pH generated the larger size, which indicated that the catalytic activity of enzymes responsible for Zn^{2+} and Ag^{2+} ions reduction appeared to be deactivated, thus causing an increase in the size and decrease in absorbance intensity of the NCs.

Furthermore, the concentration of Ag salt has a higher impact on absorbance intensity than temperature and pH, as shown in Figures 4.7 and 4.8, because of the slope of the obtained surface in the direction of the Conc.Ag salt axis is steeper than the temperature and pH axes.

By comparing Figure 4.7 with Figure 4.8, the interaction of concentration of Ag salt and temperature has a greater impact on the synthesis of ZnO-Ag NCs than that of concentration of Ag salt and pH interaction. This is in agreement with an obtained model equation where the coefficient of interaction between the concentration of Ag salt and temperature is greater than that of concentration of Ag salt and pH interaction.

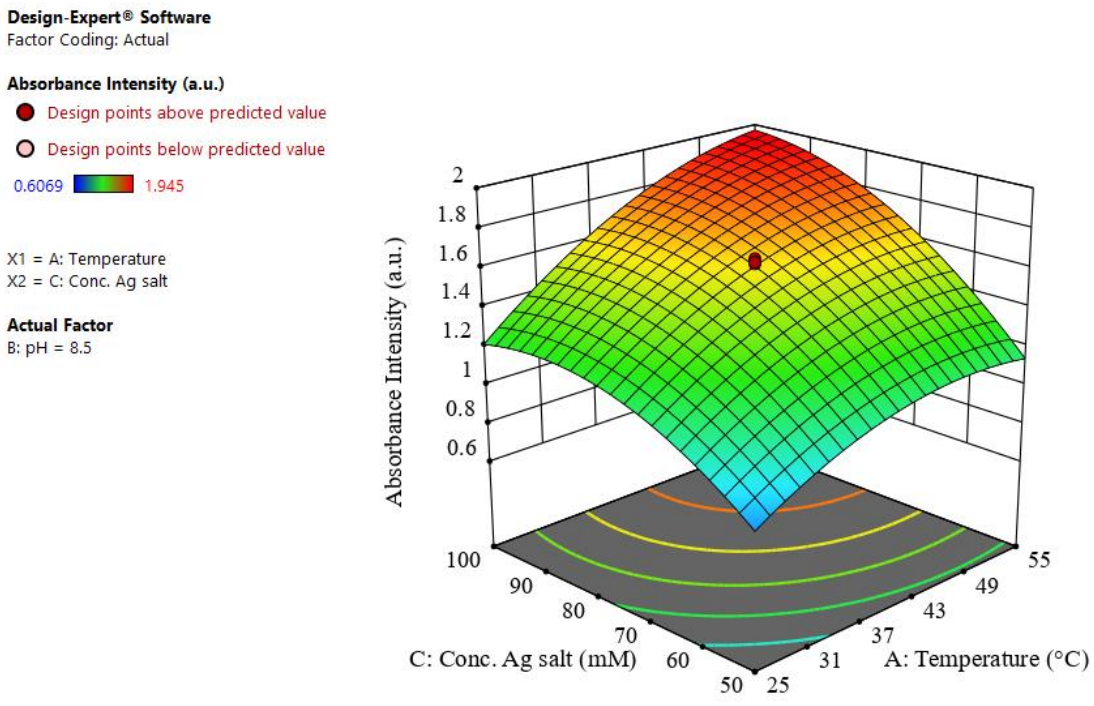

Figure 4.7 3D response plot for Conc. of Ag salt–Temperature effect on absorbance intensity.

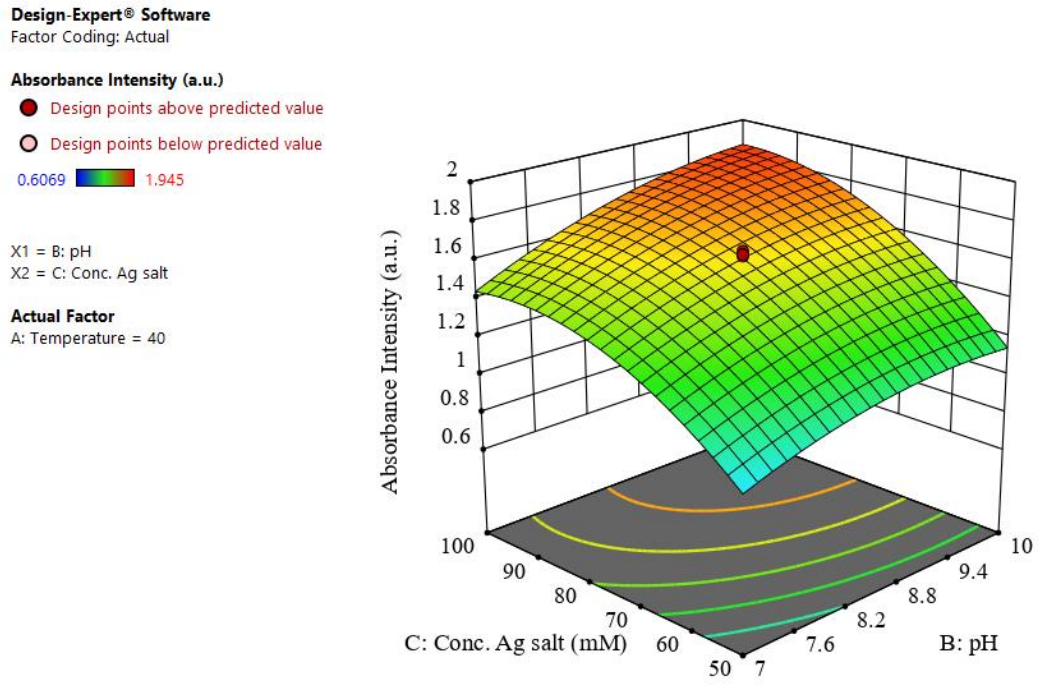

Figure 4.8 3D response surface plot for Conc. of Ag salt–pH effect on absorbance intensity.

4.2.4 Optimal process factors of synthesis

The optimal synthesis conditions were discovered using a multi-response approach after the development and validation of multivariate quadratic models. It was assumed that the absorbance intensity would be maximized while having the maximum amount of ZnO-Ag NCs with smaller sizes. Temperature = 53.7 °C, pH = 8.8, and V_{Ag} = 91.5 mL were found to be the predicted optimal conditions. From the optimum possible conditions, this was selected by taking the high cost of silver nitrate salt into consideration. Besides, the high concentration of Ag salt could result in a large size of ZnO-Ag NCs because of agglomeration.

Table 4.5 Summary of constraints and goals of optimizations

Name	Goal	Lower Limit	Upper Limit	Importance
A: Temperature	is in range	25	55	3
B:pH	is in range	7	10	3
C: Conc. Ag salt	is in range	50	100	3
Absorbance Intensity	maximize	0.6069	1.945	3

Table 4.6 Optimum possible conditions for ZnO-Ag NCs absorbance intensity

Number	Temperature	pH	Conc. Ag salt	Absorbance Intensity	Desirability	
1	**53.709**	**8.794**	**91.454**	**1.951**	**1.000**	**Selected**
2	54.735	8.555	93.039	1.947	1.000	
3	55.000	10.000	100.000	2.039	1.000	
4	48.426	9.284	96.345	1.963	1.000	
5	54.617	8.411	96.675	1.950	1.000	
6	51.909	8.636	96.269	1.950	1.000	
7	53.171	8.643	96.589	1.962	1.000	
8	49.290	9.914	97.387	1.996	1.000	
9	50.210	8.997	96.448	1.964	1.000	
10	51.747	8.625	99.895	1.955	1.000	

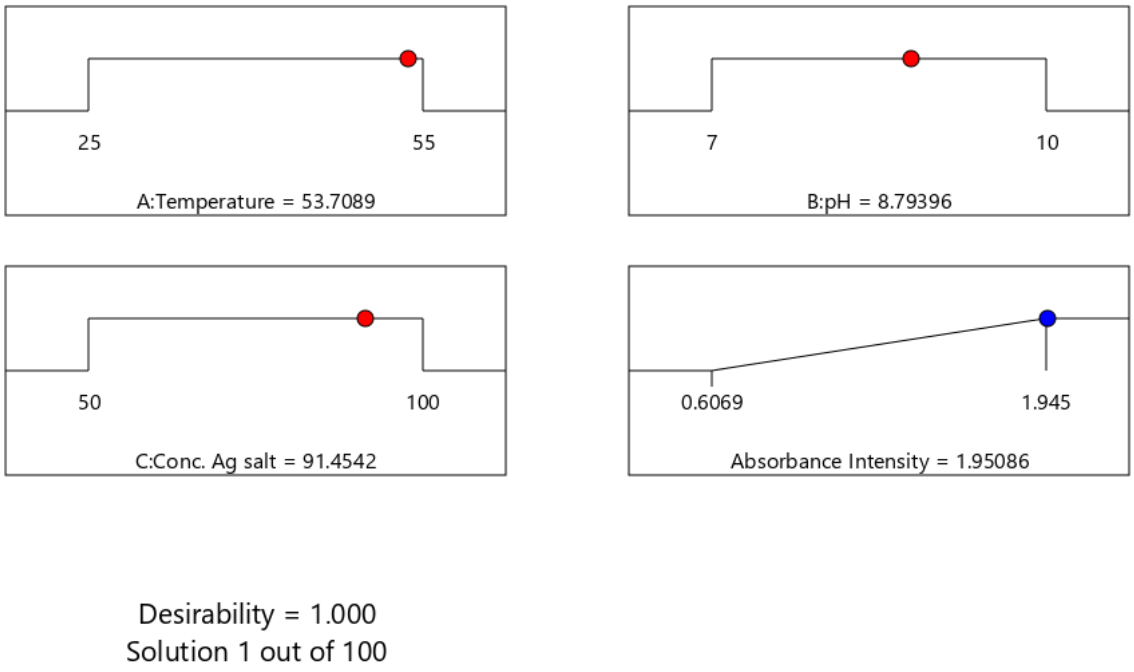

Figure 4.9 Desirability ramp for the optimization of the response and the parameters

4.2.5 Model Validation

To confirm the accuracy of the predicted optimal conditions, an actual validation experiment of ZnO-Ag NCs was carried out at Temperature = 53.7 °C, pH = 8.8, and Conc.$_{Ag}$ = 91.4 mM and the obtained UV-Vis spectra from the synthesized nanocomposite are shown in Figure 4.9. From the synthesized NCs, good absorbance spectra were obtained. The relative error for predicting absorbance intensity in synthesis run in optimal conditions, was 2.03% as given in table 4.7.

Table 4.7 Model validation for optimization of response variable

Temperature	pH	Concentration of $AgNO_3$ salt	Actual Value	Predicted Value	% Error	% Accuracy
53.7	8.8	91.4	1.905 ± 0.04	1.951	2.35	97.65

For the best conditions, this result shows that the model's predicted values and experimental values are in good agreement. Because the deviation value is less than 5%, the model that has been

obtained by response surface methodology (RSM) can be accepted. These findings support *B.Polystachya* extract's ability to biosynthesize ZnO-Ag NCs with high repeatability, as well as the possibility of controlling conditions using a mathematical approach.

4.3 Characterization of the synthesized ZnO NPs and ZnO-Ag NCs

The formation of ZnO NPs and ZnO-Ag NCs was confirmed using UV-Visible spectroscopy, XRD, FT-IR spectroscopy, and DLS which were frequently used to characterize the synthesized metal oxide nanomaterials.

4.3.1 UV–Visible Spectroscopy

UV-Vis spectroscopy was used to determine the optical absorption of ZnO NPs and ZnO-Ag NCs at room temperature. The UV visible spectroscopy of ZnO NPs and ZnO-Ag NCs is shown in Figure 4.10. Between 289 and 293 nm for ZnO and 289 nm for ZnO–Ag, there is a sharp peak that is characteristic of the polyphenolic compounds that acted actively during the synthesis and reduction processes between *B.polystachya* phytocompounds and metal precursors (Varadavenkatesan *et al*., 2019). These peaks also indicated the presence of ZnO nanoparticles, which is much shorter than the bandgap wavelength (Talam *et al*., 2012). The formation of zinc nanomaterials was confirmed by the appearance of distinct low-absorption-intensity peaks on the spectra of ZnO NPs and ZnO–Ag NCs between 330 and 390 nm, which could be due to an electron transition from the valence to the conduction band. The maximum absorption peak of ZnO-Ag NCs was 368 nm, whereas the bulk ZnO had a peak at 366 nm in the UV–Vis spectrum with their corresponding absorbance intensity 1.905 and 2.073 respectively. Different authors reported the maximum absorbance peak for ZnO NPs and ZnO-Ag NCs. Sali *et al*. (2021) reported the maximum absorption peak for ZnO-Ag NCs and ZnO NPs at 372 nm and 365 nm respectively. Zare *et al*. (2018) also reported an absorbance peaks at 381 nm and 373 nm for ZnO-Ag NCs and ZnO NPs respectively. The inclusion of Ag^{2+} in the matrix of the nano-composites was indicated by a reduction in peak intensity in the spectra of the ZnO–Ag, implying some level of agglomeration with irregular shapes (B. Kumar *et al*., 2017).

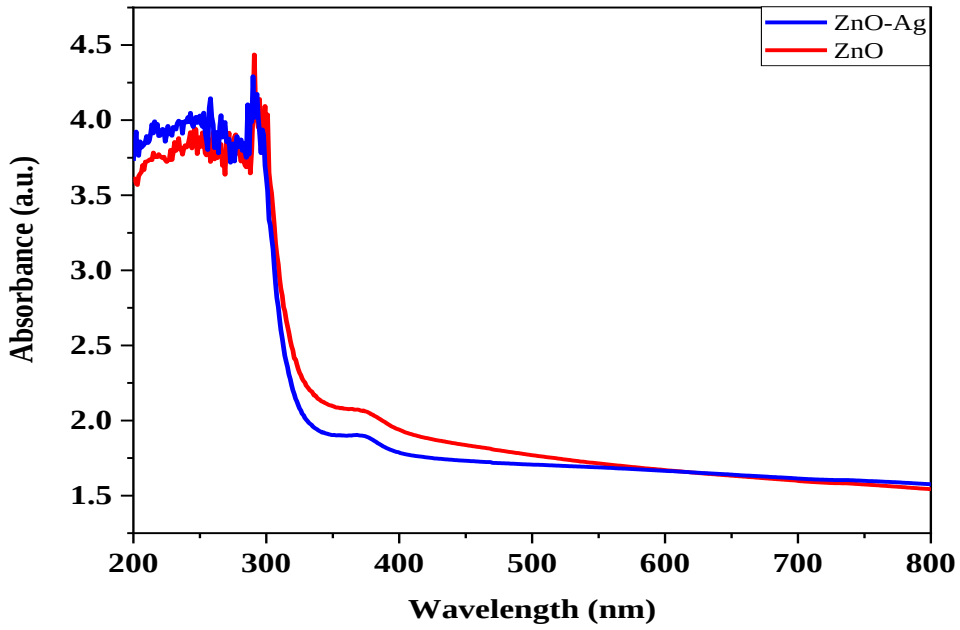

Figure 4.10 Absorbance intensity of ZnO NPs and ZnO-Ag NCs

The values of band gap energy (Eg) for synthesized nanoparticles and nanocomposites were calculated from the UV–vis spectra. Accordingly, the ZnO NPs have high bandgap energy of 3.39 eV. The bandgap for ZnO–Ag was narrowed to 3.37 eV after Ag impurities were added to the nanocomposite. This is in agreement with the results obtained by Zare *et al*. (2018). As Zn^{2+} was gradually replaced by Ag^{2+} in the matrix of the materials, the bandgap narrowed, resulting in a systematic increase in the number of oxygen vacancies due to their ion radii and electronegativity (Adhikari *et al*., 2015).

Table 4.8 UVvis absorption data for ZnO NPs and ZnO-Ag NCs.

Sample	λ (nm)	Absorbance Intensity (a.u)	Band gap (eV)
ZnO NPs	366	2.073	3.39
ZnO-Ag NCs	368	1.905	3.37

As can be observed from Table 4.8, the band gap energy of ZnO-Ag NCs is smaller than that of pure ZnO NPs. Decreasing the energy gap may be due to the presence of p-type conductivity in the ZnO-Ag NCs. Addition of Silver ion in ZnO results in the nanocomposite band in the energy

gap, which could be due to the formation of the p-type in this substance. It should be mentioned that this reduction in energy gap led to increase efficiency in the use of these materials in antibacterial activities (Hosseini *et al*., 2015).

4.3.2 X-ray Diffraction (XRD)

Powder X-ray diffraction measurements revealed the XRD patterns of the synthesized ZnO NPs and ZnO–Ag NCs. The XRD pattern of ZnO NPs and ZnO–Ag NCs is shown in Figure 4.11. Initially, the difractogram indicates the formation of wurtzite structure of pure ZnO NPs and ZnO-Ag NCs. The narrow, sharp, and strong diffraction peaks are an indication of good crystallinity of the synthesized nanomaterials. XRD difractogram revealed that the obtained materials are perfectly crystalline and single-phase, but in the case of ZnO-Ag, there observed secondary phases as well. The main characteristic peaks for ZnO NPs were found at 2θ values of 31.86°, 34.352°, 36.36°, 47.68°, 56.74°, 63.00°, 66.58°, 68.14°, and 69.20°, which belonged to the crystallographic planes of (100), (002), (101), (012), (110), (013), (200), (112), and (201) respectively. These match the Hexagonal wurtzite, according to Zhou *et al*. (2007) and Schreyer *et al*. (2014). Peaks at 28.70°, 31.12°, 32.72°, and 50.82° are due to bio-organic phases on the surface of the particles, which would have been contributed by polyphenolic compounds (B. Kumar *et al*., 2017). The crystallography of ZnO–Ag revealed peaks at 32.09°, 34.63°, 36.55°, 38.41°, 44.59°, 47.87°, 56.91°, 63.21°, 64.77°, 68.35°, 69.11°, and 77.64° and within the crystallographic planes of (110), (002), (101), (111), (200), (012), (110), (013), (202), (112), (201), and (311) respectively. The main characteristic peaks at 2θ 38.41°, 44.59°, 63.21°, and 77.64° indicates the formation of Ag^{+} signals which is close to the report by Zare *et al*. (2018). This proves that Ag^{+} is present in the ZnO–Ag NCs. Due to the substitution of Ag^{+} ions for Zn^{2+} in the ZnO lattice, there is a slight shift of peaks when Ag is added to ZnO (Singh *et al*., 2017). The substitution of Ag ion causes the shifting of diffraction peak towards lower intensity due to the fact that the ionic radii of Silver (Ag^{+} =1.22Å) are higher than that of Zn (Zn^{+2}=0.74Å) causing an increase in the unit cell volume (Khan *et al*., 2020). All of the other peaks in the XRD graph of the ZnO–Ag nanocomposite are ZnO nanoparticles. The extra peaks at 28.93°, 31.33°, 32.87°, and 40.09° are phytoconstituents from plants that may have escaped washing of ZnO–Ag during synthesis.

The significant crystallinity of ZnO and ZnO–Ag nanomaterials was confirmed by highly absorbed diffraction peaks. The presence of other diffracted peaks on the difractograms of ZnO and ZnO–

Ag confirms the presence of impurities during nanomaterial synthesis (Varadavenkatesan *et al*., 2019). The formation of ZnO-Ag NCs was indicated by the secondary phase of Ag diffraction peaks. The presence of Ag incorporated into the Zn site is confirmed by a change in crystallite size and a shift in ZnO on the difractogram (S. Kumar *et al*., 2015). These changes could be caused by interactions between the metal ions of Zn^{+} and Ag^{+} (Ag, Zn, and CH3COO-), which cause the ions to be displaced from their lattice positions (Abutalib & Rajeh, 2020).

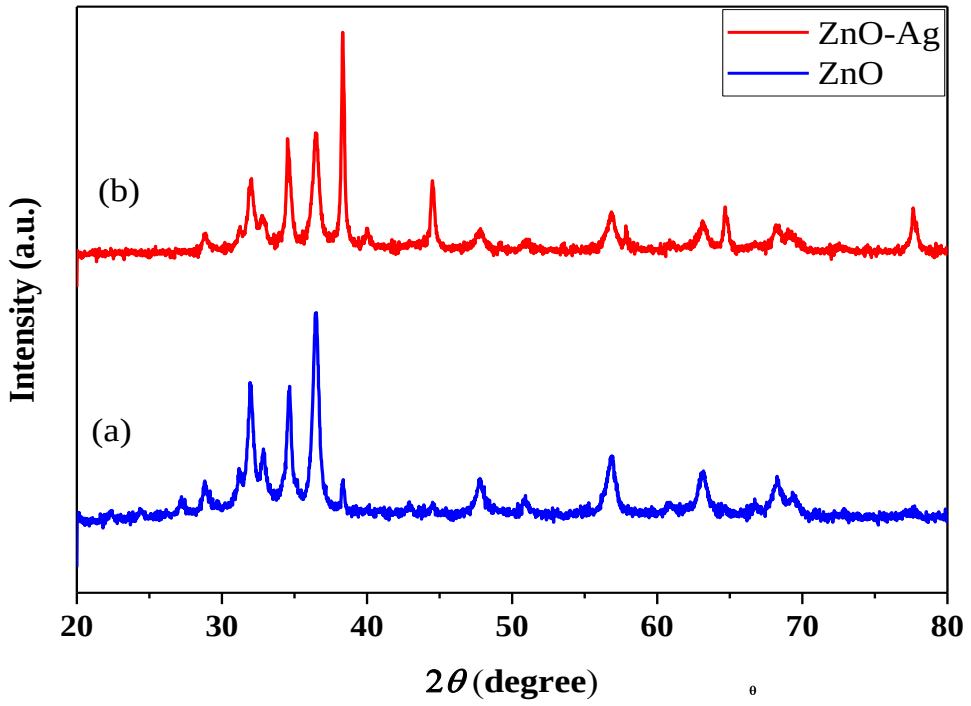

Figure 4.11 The X-ray Diffraction of ZnO NPs **(a)** and ZnO–Ag NCs **(b)**

The average crystallite size of the nanomaterials was calculated using Debye Scherer's equation (Xu et al., 2008);

$$D = \frac{0.94\lambda}{\beta \cos\theta} \qquad 4.2$$

where D is the Crystal size (nm), λ is the wavelength of the XRD used, β is full width half maximum (FWHM), and θ is Bragg's angle. The X-ray difractogram of ZnO nanoparticles and ZnO–Ag nanocomposite materials were analyzed to obtain information about various crystalline aspects. ZnO and ZnO–Ag crystallite sizes were approximately 24.50 nm and 23.55 nm,

respectively. The addition of silver salt to zinc salt resulted in a reduction in the size of nanoparticles. Many researches have noticed that adding Ag salt reduces the size of NCs when compared to ZnO NPs when introduced into the medium (Nadeem *et al*., 2019). The summary of FWHM values, the Miller indices, and the average crystallite size for the biosynthesized ZnO NPs and ZnO-Ag NCs are given in Tables 4.9 and 4.10 below.

Table 4.9 FWHM values, average crystallite sizes, and Miller indices of ZnO NPs

h k l	2θ(degree)	*d*-spacing ($d_{h\,k\,l}$)	ZnO FWHM (degree)	Crystallite Size (nm)
100	31.86	2.8100	0.3200	26.98
002	34.52	2.5985	0.4000	21.73
101	36.36	2.4717	0.4000	21.84
012	47.68	1.9077	0.4000	22.69
110	56.74	1.6218	0.5600	18.84
013	63.00	1.4753	0.7200	14.32
200	66.58	1.4048	0.2400	41.37
112	68.14	1.3764	0.6000	16.7
201	69.20	1.3583	0.2800	36.01
Average Crystal Size				24.50

Table 4.10 FWHM values, average crystallite sizes, and Miller indices of ZnO-Ag NCs

h k l	2θ(degree)	*d*-spacing ($d_{h\,k\,l}$)	ZnO-Ag FWHM (degree)	Crystallite Size (nm)
110	32.09	2.7889	0.4800	17.99
002	34.63	2.5900	0.3600	24.15
101	36.55	2.4584	0.4400	19.87
111	38.41	2.3432	0.2400	36.63
200	44.59	2.0323	0.3200	28.04
012	47.87	1.9009	0.5200	17.46
110	56.91	1.6177	0.6400	14.75
013	63.21	1.4714	0.5200	18.74
202	64.77	1.4390	0.2400	35.10
112	68.35	1.3700	0.6400	15.67
201	69.11	1.3590	0.4800	20.99
311	77.64	1.2289	0.2800	33.29
Average Crystal Size				23.55

4.3.3. Fourier Transform Infrared (FTIR) Spectroscopy

The interaction of metal salts with biological components mediates the reduction of metal ions to biosynthesized nanoparticles. The key biomolecules that influence the reduction and capping of nanoparticles include phenolic, alcoholic chemicals, flavones, polysaccharides, amino acids, alkaloids, terpenoids, enzymes, and proteins (Abdullah *et al*., 2020). *B.polystachya* is mostly made up of triterpenoids, iridoids, flavonoids, and phenylethanoids, alkaloids, terpenoids, cardiac glycosides, oils, saponin compounds, and other bioactive substances, according to researches (Tai *et al*., 2011; Kahsay, 2017). Table 4.1 lists some of the primary chemical elements of leaf extract *B.polystachya* that were analyzed in this investigation. As a result, the functional groups linked to these organic materials may be involved in the reduction of metal salts ($Zn(CH3COO)_2$ and $AgNO_3$) to ZnO NPs and ZnO-Ag NCs, as well as capping the products.

The possible functional groups that are actively involved in the reduction of $Zn(CH_3COO)_2$ and $AgNO_3$ to various nanoparticles and nanocomposite were identified using FTIR as shown in figure 4.12. Hydrogen O–H band stretching was assigned to a broad peak on the spectra of ZnO

NPs and ZnO–Ag NCs at 3401 and 3425 cm^{-1} respectively. This could be due to water's hydroxyl groups (Zamiri *et al*., 2014). Both ZnO NPs and ZnO–Ag NCs have a crest at 1547 cm^{-1} which is characteristic of symmetric stretch of C-C in aromatic rings (Jamdagni *et al*., 2016).

The ZnO NPs have a peak at 1082 cm^{-1} for C-N stretches (Ogunyemi *et al*. 2019). Amine N-H vibrational stretch was confirmed by spectral bands at 1440 cm^{-1} for both ZnO and ZnO–Ag nanomaterials. The peaks at 748 and 838 cm^{-1} are attributed to the presence of the C-H bend in the alkane group (Jamdagni *et al*., 2016). The peak at 545 is the characteristic band of the ZnO NPs. The FTIR spectrum, absorption at 400 cm^{-1} to 600 cm^{-1} identifies the presence of ZnO NPs (Ogunyemi *et al*. 2019) which further confirms the formation of ZnO NPs and ZnO-Ag NCs by using *B.polystachya* leaf extract.

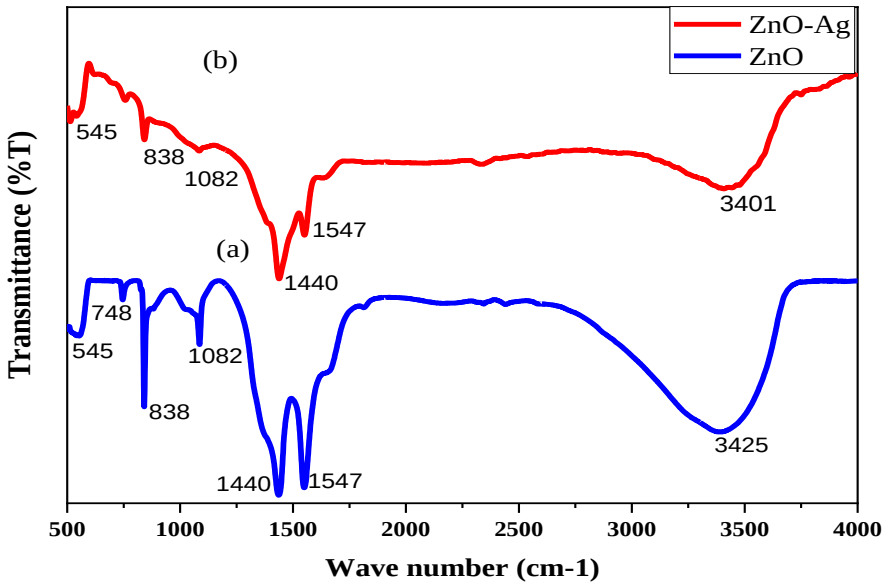

Figure 4.12 FTIR of ZnO NPs **(a)** and ZnO–Ag NCs **(b)**

The coordination of ZnO NPs with –OH and C=O groups may be responsible for the stability and capping agent of produced ZnO NPs. It's also possible to deduce that the reduction process is caused by the presence of phenolic and flavonoid group molecules (Ahmad & Kalra, 2020). On the FT-IR spectra, the absence of S=O, C-O stretches, and H-C-H asymmetric bands confirmed that the functional groups were used up in the reduction of zinc acetate and silver nitrate. All of

the bands and functional groups discovered are unique to the phytoconstituents discovered through phytochemical screening (Gurgur *et al*., 2020).

4.3.4 Dynamic Light Scattering (DLS)

Using DLS as a standard particle size analyzer, the size and size distribution of the obtained ZnO NPs and ZnO-Ag NCs in the optimum conditions were evaluated. As shown in Figure 4.13, 100 percent of ZnO NPs had a size of 74.91 nm. Similarly, 11.1% of ZnO-Ag NCs were 18.6 nm in size and 88.9% percent were 37.69 nm in size. The variation in ZnO-Ag NCs sizes could be attributed to the poly-disperse nature of nanoparticles as indicated by the polydispersity index (PDI) value of 0.6. PDI is a term used to describe a distribution's degree of "non-uniformity," which in the case of nanoparticle suspensions could be related to the occurrence of nanoparticles as aggregates or agglomerates, resulting in variability in calculated particle size compared to actual particle size. Reportedly, PDI is dimensionless and scaled such that values smaller than 0.05 are mainly seen with highly monodisperse standards and values bigger than 0.7 indicate that the sample has a very broad particle size distribution (Iqtedar *et al*., 2020; Danaei *et al*., 2018).

The Z-average particle size given by the instrument was 78.69 nm and 35.48 nm for ZnO NPs and ZnO-Ag NCs respectively. This confirms that the biosynthesized nanoparticles are on the nanometer scale. It is also in agreement with the report by Jamdagni *et al*. (2016) in which the average size of ZnO NPs was found 74.36 nm with a unimodal peak. Moreover, sizes of ZnO NPs were reported as 82.31 nm with PDI values of 0.262 in other study (Iqtedar *et al*., 2020).

Table 4.11 The average particle size of ZnO NPs and ZnO-Ag NCs from the DLS instrument.

Nanomaterial		Size (d.**nm**)	% Intensity	PDI	Z-average (nm)
ZnO NPs	Peak 1	74.91	100	0.05	78.69
	Peak 2	0.000	0.0		
	Peak 3	0.000	0.0		
ZnO-Ag NCs	Peak 1	37.69	88.9	0.6	35.48
	Peak 2	3.757	11.1		
	Peak 3	0.000	0.0		

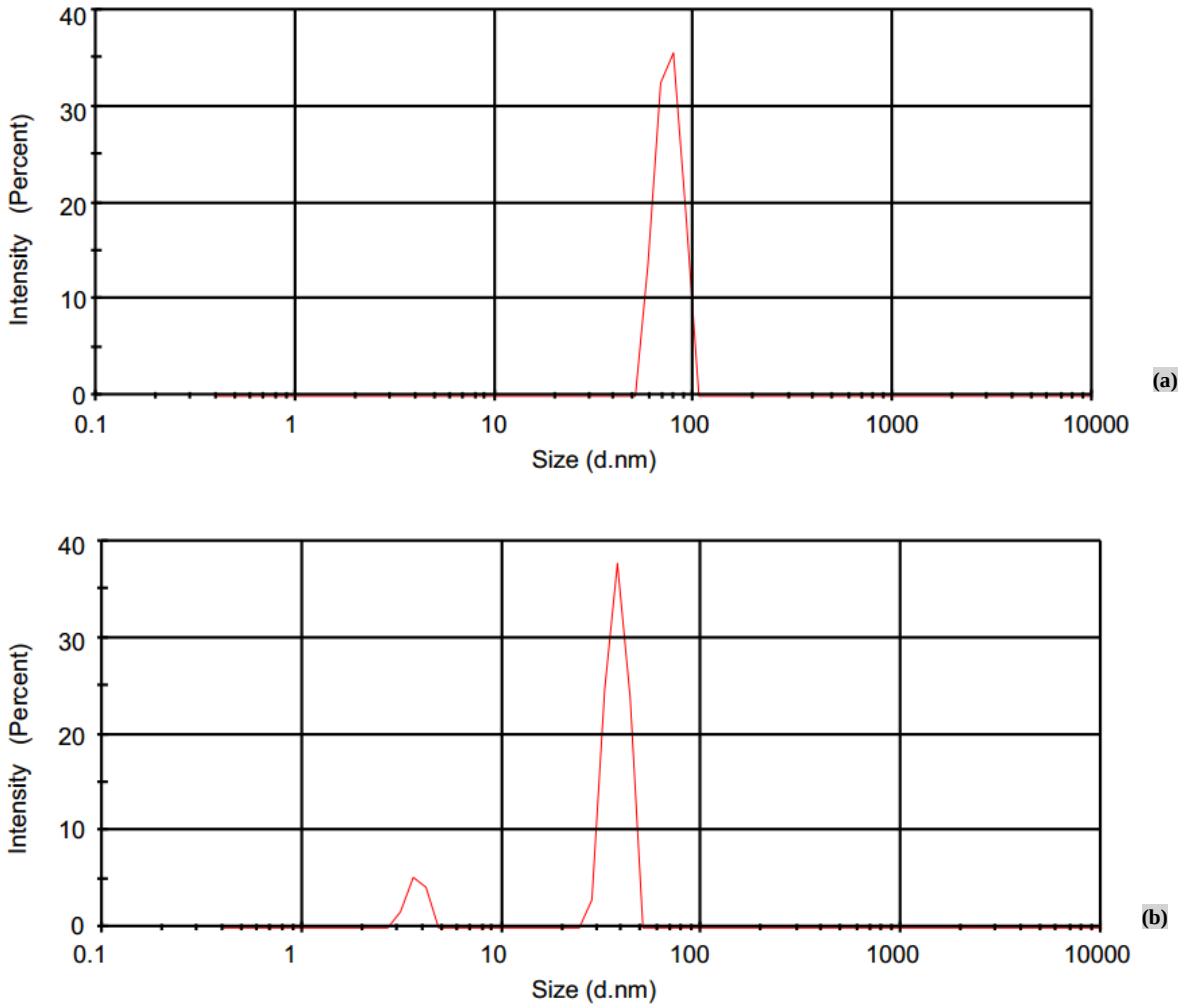

Figure 4.13 Size distribution of ZnO NCs (a) and ZnO-Ag NCs (b)

Therefore, by comparing the above two results, we can conclude that ZnO with dopant $AgNO_3$ is very appropriate since it gives the lowest average size of nanoparticles.

4.4 Antibacterial Activity

The antimicrobial effects of the green-synthesized ZnO NPs and ZnO-Ag NCs were investigated first using disc diffusion method against *S.aureus* and *E.coli*. The free zone of inhibition diameter is illustrated in table 4.12 and figure 4.14. It has been observed that both nanomaterials have moderate bactericidal properties towards both the bacterial strains studied when compared to the reference drugs. The dimethyl sulfoxide (DMSO) and gentamicine were used as negative and positive control respectively against both the bacterial strains. The result shows higher antibacterial activity against *E.coli* (ZnO-Ag: 15 ±0.31 mm and ZnO-NPs: 13 ±0.36 mm) followed by moderate

activity against *S.aureus* (ZnO-Ag: 8 ±0.37 mm and ZnO-NPs: 7 ±0.25 mm) at the concentration of 500 mg/mL.

The effectiveness of the green synthesized zinc nanomaterials in the tested bacterial strains was determined by measuring the minimum inhibitory concentration (MIC). As a result, MIC values between 62.5–250 mg/mL were obtained for both the biosynthesized nanomaterials against the two bacterial strains. The results of MIC as shown in Table 4.12 exhibited that both *S.aureus* and *E.coli* were susceptible to the minimum inhibitory concentration of ZnO-Ag NCs at 125 and 62.5 mg/mL respectively. On the other hand, the MIC of ZnO NPs for *S.aureus* and *E.coli* was observed at 250 and 125 mg/mL respectively. An inhibition zones of 7 ±0.24 and 8 ±0.05 mm were recorded by the MIC of ZnO-Ag NCs for *S.aureus* and *E.coli* respectively. Similarly, the MIC of ZnO NPs had induced an inhibition zones of 7±0.12 and 7±0.042 mm against *S.aureus* and *E.coli* respectively. Based on the results obtained from MIC and disc diffusion methods, it can be suggested that in comparison with gram-negative bacteria, the growth of Gram-positive bacteria is inhibited at higher concentrations of ZnO NPs and ZnO-Ag NCs.

From the results it was observed a significant difference between antibacterial activity of ZnO NPs and ZnO-Ag NCs. The differences in antibacterial activity between the nanomaterials can be drawn in different ways. First, the morphology and other physiological characteristics of the nanomaterials. Smaller nanoparticles have the potential to enter cells and cause harm. In this study, ZnO-Ag NCs have smaller particle size and a higher surface-to-volume ratio than ZnO NPs. Because of their smaller size, ZnO-Ag NCs can easily penetrate bacterial cells and have a better bactericidal effect. Secondly, the physiological, morphological, and biochemical characteristics of strains that distinguish Gram-positive from Gram-negative strains (Nadeem *et al*., 2019).

According to the findings, bacterial sensitivity to nanomaterials varies depending on the antimicrobial species. As can be seen from the data, gram-negative bacteria are more sensitive to ZnO NPs and ZnO-Ag NCs treatments than gram-positive bacteria, which could be due to the latter group's cell walls having a thick coating (peptidoglycan). Gram-negative bacteria are more susceptible than gram-positive bacteria, according to a previous study. They came to the conclusion that gram-positive bacteria's resistance is due to a thick layer of peptidoglycan in their cell wall (Umar *et a*l., 2019), which is similar to the findings in this study.

Table 4.12 Zone of inhibition (mm) of ZnO NPs and ZnO-Ag NCs against Gram-positive and Gram-negative bacterial strains.

Samples	*S.aureus* (gram-positive)			*E.coli* (gram-negative)		
	Zone of Inhibition (mm) (diameter)	Percent activity index (%)	MIC (mg/ml)	Zone of Inhibition (mm)	Percent activity index (%)	MIC (mg/ml)
ZnO-Ag NCs	8±0.37	40	125	15±0.31	71.4	62.5
ZnO NPs	7±0.25	35	250	13±0.36	62	125
Gentamicine	20±0.20			21±0.25		
DMSO	NA			NA		

NA= not active

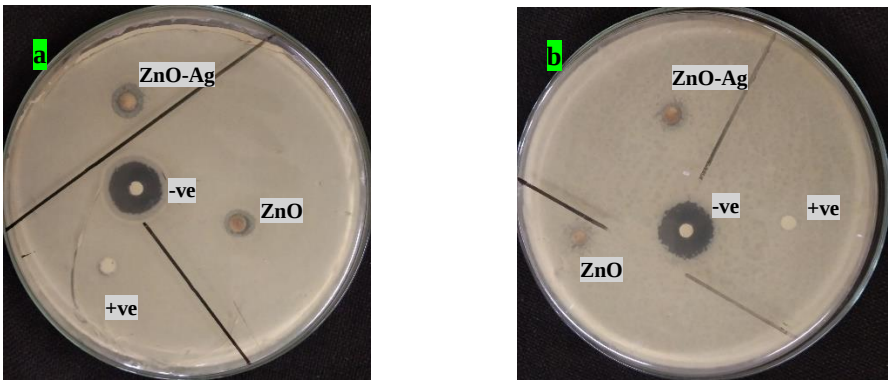

Figure 4.14 Evaluation of antibacterial activity of ZnO NPs and ZnO-Ag NCs against *Escherichia coli* **(a)** and *Staphylococcus aureus* **(b)**

Based on the findings, it can be concluded that doping ZnO with Ag could enhance bactericidal activity. Smaller size and a sufficient amount of bioactive compounds adsorbed on ZnO-Ag NCs resulted in increased antibacterial efficacy. Besides, moderate activity concludes that the more susceptible bacteria was *Eschesheria Coli* and more resistant was *Staphylococcus aureus*.

5. CONCLUSION AND RECOMMENDATION

5.1 Conclusion

In this study, ZnO nanoparticles and ZnO-Ag nanocomposites were made using a simple, cost-effective, and environmentally friend green method involving *B.polystachya* plant extract (Anfar) as a reducing, stabilizing, and capping agent. CCD was used to optimize the experimental conditions of the biosynthesis process of ZnO-Ag NCs using herbal extracts. The absorbance intensity of the ZnO-Ag NCs was used as the response in this approach, and the interaction of factors as well as the original factors (temperature, pH, and Conc. Ag salt) was used as dependent variables during the NCs optimization. The efficiency of CCD in the biosynthesis of ZnO-Ag NCs was demonstrated by a quadratic model with R^2=0.9875 and statistical significance in ANOVA, as well as a non-significant lack of fit. The ZnO-Ag NCs were prepared under optimum conditions (Temp = 53.7 °C, pH = 8.8, Conc. Ag salt = 91.4 mM). The FTIR spectrum revealed that the main possible adsorbed compounds on the ZnO NPs and ZnO-Ag NCs' surface were polyphenolic molecules. DLS confirmed that 100 percent of ZnO NPs had a size of 74.91 nm. Similarly, 11.1% of ZnO-Ag NCs were 18.6 nm in size and 88.9% percent were 37.69 nm in size. The Z-average particle size given by the instrument was 78.69 nm and 35.48 nm for ZnO NPs and ZnO-Ag NCs respectively, which confirms that the biosynthesized nanoparticles are on the nanometer scale. The ability of the *B.Polystachya* leaf extract to reduce Zn^+ and Ag^+ and prepare ZnO NPs and ZnO-Ag NCs with average crystalline sizes of 24.50 and 23.55nm, respectively, was also confirmed by XRD. The size and crystalline size of ZnO-NPs were reduced by doping ZnO with Ag. This is also, to our knowledge, the first study of the antibacterial activity of ZnO NPs and ZnO-Ag NCs synthesized by *B.Polystachya* leaf extract, which showed moderate activity against *S. aureus* and *E. coli*. When compared to pure ZnO-NPs, the ZnO-Ag nanocomposite has more bactericidal effects. Green synthesis of ZnO NPs and ZnO-Ag NCs can be considered an alternative method of synthesis because it is cost-effective, environmentally friendly, and compatible with human health due to less waste and safer products. The product can be used in various medical applications in future studies due to the safe synthesis process and confirmed antibacterial activities of ZnO NPs and ZnO-Ag NCs synthesized by *B.Polystachya*. The synthesis of ZnO NPs and ZnO-Ag NCs using the proposed method, on the other hand, does not require high temperatures and can be completed in a matter of hours.

5.2 Recommendations

In this study, ZnO NPs and ZnO-Ag NCs were synthesized using *B.polystachya* leaf extract. The effect of temperature, pH, and concentration of Ag salt on the absorbance intensity of ZnO-Ag NCs has been studied and optimized. Moreover, the crystal size, absorbance intensity, bandgap, functional groups, and size distribution of the nanomaterials were characterized. Finally, the bactericidal effect of the nanomaterials was studied against two bacterial strains. Therefore, based on the results of this study it is recommended that:

- In vitro and in vivo biological studies should be done to assess the potential cytotoxicity, biosafety, and biocompatibility of the nanomaterials.
- Further research should be done to investigate the thermal stability and morphology of synthesized nanoparticles and nanocomposites.
- The antibacterial activity in future research should include testing against other types of bacteria's and microbes.
- The effect of plant extract volume on the synthesis of ZnO NPs and their nanocomposite should be investigated further.

REFERENCES

Abdullah, F. H., Bakar, N. H. H. A., & Bakar, M. A. (2020). Optik Low temperature biosynthesis of crystalline zinc oxide nanoparticles from Musa acuminata peel extract for visible-light degradation of methylene blue. *Optik - International Journal for Light and Electron Optics*, *206*(December 2019), 164279.

Abutalib, M. M., & Rajeh, A. (2020). Influence of ZnO/Ag nanoparticles doping on the structural, thermal, optical and electrical properties of PAM/PEO composite. *Physica B: Condensed Matter*, *578*(October), 411–419.

Adhikari, S., Banerjee, A., Eswar, N. K. R., Sarkar, D., & Madras, G. (2015). Photocatalytic inactivation of E. Coli by ZnO-Ag nanoparticles under solar radiation. *RSC Advances*, *5*(63), 51067–51077.

Ahmad, W., & Kalra, D. (2020). Journal of King Saud University – Science Green synthesis , characterization and anti microbial activities of ZnO nanoparticles using Euphorbia hirta leaf extract. *Journal of King Saud University - Science*, *32*(4), 2358–2364.

Al-kordy, H. M. H., Sabry, S. A., & Mabrouk, M. E. M. (2021). Statistical optimization of experimental parameters for extracellular synthesis of zinc oxide nanoparticles by a novel haloalaliphilic Alkalibacillus sp . W7. *Scientific Reports*, *11*, 1–14.

Al Ati, H. Y. ehy., Fawzy, G. A. hme., El Gamal, A. A. l., Khalil, A. T. ah., El Din El Tahir, K., Abdel-Kader, M. S. aa., & Gilani, A. H. (2015). Phytochemical and biological evaluation of Buddleja polystachya growing in Saudi Arabia. *Pakistan Journal of Pharmaceutical Sciences*, *28*(4), 1533–1540.

Ali, A., & Ahmed, S. (2018). *Green Synthesis of Metal , Metal Oxide Nanoparticles , and Their Various Applications*.

Aneesh, P. M., Vanaja, K. A., & Jayaraj, M. K. (2007). Synthesis of ZnO nanoparticles by hydrothermal method. *Nanophotonic Materials IV*, *6639*(2007), 66390J.

Annu, Ali, A., & Ahmed, S. (2018). Green Synthesis of Metal, Metal Oxide Nanoparticles, and Their Various Applications. In *Handbook of Ecomaterials*.

Arooj, S., Nazir, S., Nadhman, A., Ahmad, N., Muhammad, B., Ahmad, I., Mazhar, K., & Abbasi, R. (2015). Novel ZnO : Ag nanocomposites induce significant oxidative stress in human fibroblast malignant melanoma (Ht144) cells. *Journal of Nanotechnology*, *6*, 570–582.

Atsbeha, B., Mammo, F., & Kibret, B. (2017). Phytochemical Investigation on The Leaves of Buddleja Polystachya (Ethanol Extract). *International Journal of Integrative Sciences, Innovation and Technology*, *December 2014*.

Bayuo, J., Abukari, M. A., & Pelig-Ba, K. B. (2020). Optimization using central composite design (CCD) of response surface methodology (RSM) for biosorption of hexavalent chromium from aqueous media. *Applied Water Science*, *10*(6), 1–12.

Bipin, D. L., & Art, S. S. (2020). *Smart Nanosystems for Biomedicine, Optoelectronics and Catalysis*.

Danaei, M., Dehghankhold, M., Ataei, S., Hasanzadeh Davarani, F., Javanmard, R., Dokhani, A., Khorasani, S., & Mozafari, M. R. (2018). Impact of particle size and polydispersity index on the clinical applications of lipidic nanocarrier systems. *Pharmaceutics*, *10*(2), 1–17.

Demissie, M. G., Sabir, F. K., Edossa, G. D., & Gonfa, B. A. (2020). Synthesis of Zinc Oxide Nanoparticles Using Leaf Extract of Lippia adoensis (Koseret) and Evaluation of Its Antibacterial Activity. *Journal of Chemistry*, *2020*, 1–9.

Din, S. H., Shah, M. A., Sheikh, N. A., & Butt, M. M. (2019). Nano-Composites and Their Applications : A Review 4 . Structure and Properties of nanocomposites 5 . Ceramic Matrix Nanocomposites. *Characterization and Application of Nanomaterials*, *2*, 1–9.

Dinah, H., Immaculate, K., Michira, N., Mwaura, F. B., Derese, S., Feleni, U., & Iwuoha, E. I. (2019). Silver – zinc oxide nanocomposite antiseptic from the extract of Bidens pilosa. *SN Applied Sciences*, *1*(7), 1–17.

Dumbrava, A., Berger, D., Matei, C., Prodan, G., Aonofriesei, F., & Daniel, M. (2019). New Composite Nanomaterials with Antimicrobial and Photocatalytic Properties Based on Silver and Zinc Oxide. *Journal of Inorganic and Organometallic Polymers and Materials*, *0123456789*.

El-Domiaty, M. M., Aal, M. M. A., Abou-Hashem, M. M., Abd-Alla, R. H., & Wink, M. (2009). Antihepatotoxic Activity and Chemical Constituents of Buddleja asiatica Lour. *Zeitschrift Fur Naturforschung - Section C Journal of Biosciences*, *64*(1–2), 11–19.

Elmineh, T. (2019). *Green Synthesis and Characterization of Zinc Oxide (ZnO) Nanoparticles using Neem (Azadirachta Indica) Leaf Extract and Investigation of its Antibacterial Activities*.

Fan, Z., & Lu, J. G. (2005). Zinc oxide nanostructures: Synthesis and properties. *Journal of Nanoscience and Nanotechnology*, *5*(10), 1561–1573.

Fawzy, G. A., Gamal, A. A. El, & Ati, H. Y. Al. (2013). Antimicrobial and cytotoxic potentials of Buddleja polystachya extracts. *Bangladesh Journal of Pharmacology*, *8*(2), 136–141.

Forruque, S., Mofijur, M., Rafa, N., Tasnim, A., Chowdhury, S., Nahrin, M., Islam, A. B. M. S., & Chyuan, H. (2021). Green approaches in synthesising nanomaterials for environmental nanobioremediation : Technological advancements , applications , benefits and challenges. *Environmental Research*, *204*, 111967.

Getahun, A., Demelash, Z., Ambikar, D., & Asrade, S. (2021). In vivo evaluation of 80 % methanolic leaves crude extract and solvent fractions of buddleja polystachya fresen (buddlejaceae) for wound healing activity in normal and diabetic mice. *Metabolism Open*, *11*, 100–110.

Gheshlaghi, R., Scharer, J. M., Moo-Young, M., & Douglas, P. L. (2008). Application of statistical design for the optimization of amino acid separation by reverse-phase HPLC. *Analytical Biochemistry*, *383*(1), 93–102.

Golbraikh, A., & Tropsha, A. (2002). Predictive QSAR modeling based on diversity sampling of experimental datasets for the training and test set selection Alexander. *Molecular Diversity*, *2000*, 231–243.

Gour, A., & Jain, N. K. (2019). Advances in green synthesis of nanoparticles. *Journal of Artificial Cells, Nanomedicine, and Biotechnology*, *47*(1), 844–851.

Gul, R., Jan, S. U., Faridullah, S., Sherani, S., & Jahan, N. (2017). Preliminary Phytochemical Screening, Quantitative Analysis of Alkaloids, and Antioxidant Activity of Crude Plant Extracts from Ephedra intermedia Indigenous to Balochistan. *Scientific World Journal*, 1–7.

Gunnarsson, R., Helmersson, U., & Pilch, I. (2016). Synthesis of titanium - oxide nanoparticles with size and stoichiometry control. *Asian Journal of Pharmaceutical and Clinical Research*, *9*(4), 1–15.

Gupta, P. K., & Kim, B. S. (2021). Green Synthesis of Metallic Nanoparticles : Applications and Limitations. *Journal of Catalysts*, *902*(11), 1–35.

Gurgur, E., Oluyamo, S. S., Adetuyi, A. O., Omotunde, O. I., & Okoronkwo, A. E. (2020). Green synthesis of zinc oxide nanoparticles and zinc oxide – silver , zinc oxide – copper nanocomposites using Bridelia ferruginea as biotemplate. *SN Applied Sciences*, *2*(5), 1–12.

Handzlik, J., Matys, A., & Kieć-kononowicz, K. (2018). Recent Advances in Multi-Drug Resistance (MDR) Efflux Pump Inhibitors of Gram-Positive Bacteria S. aureus. *Journal of Antibiotics*, *2*, 28–45.

Hemalatha, S., & Makeswari, M. (2017). Green synthesis, characterization and antibacterial studies of CuO nanoparticles from Eichhornia crassipes. *Rasayan Journal of Chemistry*, *10*(3), 838–843.

Henderson, D. K. (2006). Managing Methicillin-Resistant Staphylococci : A Paradigm for Preventing Nosocomial Transmission of Resistant Organisms. *The American Journal of Medicinr*, *119*(6A), 45–52.

Horikoshi, S., & Serpone, N. (2013). *Introduction to Nanoparticles*.

Hosseini, S. M., Sarsari, I. A., Kameli, P., & Salamati, H. (2015). Effect of Ag doping on structural , optical , and photocatalytic properties of ZnO nanoparticles. *Journal of Alloys and Compounds*, *640*, 408–415.

Houghton, P. J. (1984). Ethnopharmacology of some Buddleja species. *Journal of Ethnopharmacology*, *11*(3), 293–308.

Hu, K., Dong, A., Sun, Q., & Yao, X. (2001). Bioactivity of 247 traditional Chinese medicines against Pyricularia oryzae. *Pharmaceutical Biology*, *39*(1), 47–53.

Igwe, O. (2018). Biofabrication of cobalt Nanoparticles using leaf extract of Chromolaena odorata and their potential antibacterial application. *Research Journal of Chemical Sciences*, *8*(1), 11–17.

Iqtedar, M., Riaz, H., Kaleem, A., Abdullah, R., Aihetasham, A., Naz, S., & Sharif, S. (2020). Biosynthesis, optimization and characterization of ZnO nanoparticles using Bacillus cereus MN181367 and their antimicrobial activity against multidrug resistant bacteria. *Revista Mexicana de Ingeniería Química*, *19*(1), 253–266.

Jamdagni, P., Khatri, P., & Rana, J. S. (2016). Green synthesis of zinc oxide nanoparticles using flower extract of Nyctanthes arbor-tristis and their antifungal activity. *Journal of King Saud University - Science*.

Jameel, M. S., Aziz, A. A., & Dheyab, M. A. (2020). Green synthesis : Proposed mechanism and factors in fl uencing the synthesis of platinum nanoparticles. *Green Processing and Synthesis*, *9*, 386–398.

Jeevanandam, J., Chan, Y. S., & Danquah, M. K. (2016). Biosynthesis of Metal and Metal Oxide Nanoparticles. *ChemBioEng Reviews*, *3*(2), 55–67.

Kalpana, V. N., & Rajeswari, V. D. (2018). A Review on Green Synthesis, Biomedical Applications, and Toxicity Studies of ZnO NPs. *Bioinorganic Chemistry and Applications*, *2018*, 1–12.

Kaper, J. B., Nataro, J. P., & Mobley, H. L. T. (2004). Pathogenic Escherichia coli. *Nature Reviews Microbiology*, *2*(2), 123–140.

Karande, A. M., Kamble, H. V, Kumbhar, V. H., Kane, S. R., Magdum, C. S., & Kane, S. R. (2016). Preliminary phytochemical screening of Glochidion ellipticum. *European Journal of Experimental Biology*, *6*(4), 41–45.

Kartopu, G., & Yalçın, O. (2010). *Fabrication and Applications of Metal Nanowire Arrays Electrodeposited in Ordered Porous Tem-plates*. INTECH Open Access Publisher, Rijeka.

Kennady, S. J., & Madhu, K. U. (2020). In fl uence of Zn concentration on zinc oxide nanoparticles and their anti-corrosion property. *Journal of Alloys and Compounds*, *834*, 155078.

Khan, S. H., Pathak, B., & Fulekar, M. H. (2020). A study on the influence of metal (Fe , Bi , and Ag) doping on structural , optical , and antimicrobial activity of ZnO nanostructures. *Advanced Composites and Hybrid Materials*, *24*, 324–343.

Kulkarni, S. S. (2015). *Optical and Structural Properties of Zinc Oxide Nanoparticles*. *2*(1), 14–18.

Kumar, B., Smita, K., Cumbal, L., & Debut, A. (2017). Green synthesis of silver nanoparticles using Andean blackberry fruit extract. *Saudi Journal of Biological Sciences*, *24*(1), 45–50.

Kumar, S., Singh, V., & Tanwar, A. (2015). Structural , morphological , optical and photocatalytic properties of Ag-doped ZnO nanoparticles. *Journal of Materials Science: Materials in Electronics*, 1–8.

Leeuwenberg, A. J. M. (1979). *THE LOGANIACEAE OF AFRICA XVIII Buddleja L . II: Revision of the African and Asiatic species* (Vol. 4, Issue 5).

López, A., Acosta, D., I. Martínez, A., & Santiago, J. (2010). Nanostructured low crystallized titanium dioxide thin films with good photocatalytic activity. *Powder Technology*, *202*(1–3), 111–117.

Masalha, M., Borovok, I., Schreiber, R., Aharonowitz, Y., & Cohen, G. (2001). Analysis of Transcription of the Staphylococcus aureus Aerobic Class Ib and Anaerobic Class III Ribonucleotide Reductase Genes in Response to Oxygen. *Journal of Bacteriology*, *183*(24), 7260–7272.

Mohanraj, V. J., & Chen, Y. (2006). Nanoparticles – A Review. *Tropical Journal of Pharmaceutical Research*, *5*(June), 561–573.

Nadeem, A., Naz, S., Sarfraz, J., Mannan, A., & Zia, M. (2019). Synthesis , characterization and biological

activities of monometallic and bimetallic nanoparticles using Mirabilis jalapa leaf extract. *Biotechnology Reports*, *24*, e00338.

Nikaeen, G., Yous, S., Rahmdel, S., & Samari, F. (2020). Central Composite Design for Optimizing the Biosynthesis of Silver Nanoparticles using Plantago major Extract and Investigating Antibacterial , Antifungal and Antioxidant Activity. *Scientific Reports*, *9642*(10), 1–16.

Ogunyemi, S. O., Abdallah, Y., Zhang, M., Hong, X., Ibrahim, E., Masum, M. I., Mo, J., & Li, B. (2019). Green synthesis of zinc oxide nanoparticles using different plant extracts and their antibacterial activity against Xanthomonas oryzae pv . oryzae. *Artificial Cells, Nanomedicine, and Biotechnology*, *47*(1), 341–352.

Oluyamo, E. G. S. S., & Omotunde, A. O. A. O. I. (2020). Green synthesis of zinc oxide nanoparticles and zinc oxide – silver , zinc oxide – copper nanocomposites using Bridelia ferruginea as biotemplate. *SN Applied Sciences*, *2*(5), 1–12.

Patra, J. K., & Baek, K. (2014). Green Nanobiotechnology : Factors Affecting Synthesis and Characterization Techniques. *Journal of Nanomaterials*, *2014*, 1–12.

Ramani, M., Ponnusamy, S., & Muthamizhchelvan, C. (2012). Zinc oxide nanoparticles: A study of defect level blue-green emission. *Optical Materials*, *34*(5), 817–820.

Rehman, N. U., Gilani, A. H., Khan, A., Nazneen, M., El Gamal, A. A., Fawzy, G. A., Al-Ati, H. Y., & Abdel-Kader, M. S. (2015). Antidiarrheal and Antispasmodic Activities of Buddleja polystachya are Mediated Through Dual Inhibition of Ca++ Influx and Phosphodiesterase Enzyme. *Phytotherapy Research*, *29*(8), 1211–1218.

Rezaei-zarchi, S., Javed, A., Ghani, M. J., Firouzabadi, F. B., Moghaddam, A. B., & Mirjalili, S. H. (2010). Ar ch ive. *Iran Journal of Pathology*, *5*(2), 83–89.

Sali, R. K., Pujar, M. S., Patil, S., & Sidarai, A. H. (2021). Green Synthesis of ZnO and Ag-ZnO Nanoparticles using Macrotyloma Uniflorum : Evaluation of Antibacterial Activity. *Advanced Materials Letters*, *12*(7), 1–7.

Sarah, S., Ismail, M., & Rahmahwati, A. (2019). Effect of annealing temperature on the properties of transition metal doped zinc oxide – A review. *AIP Conference Proceedings*, *020101*(February), 2068.

Schreyer, M., Guo, L., Thirunahari, S., Gao, F., & Garland, M. (2014). Simultaneous Determination of Several Crystal Structures from Powder Mixtures – The Combination of PXRD , BTEM and Rietveld

Methods. *Applied Crystallography*, 659–667.

Selim, A. K., Khalil, E. K., Abdel-Bary, S. M., & Abdel-Azeim, A. N. (2008). Extraction, Encapsulation and Utilization of Red Pigments from Roselle (Hibiscus sabdariffa L.) as Natural Food Colourants. *Alexandria Journal of Food Science and Technology*, *5*(2), 7–20.

Shabaani, M., Rahaiee, S., Zare, M., & Mahdi, S. (2020). Green synthesis of ZnO nanoparticles using loquat seed extract ; Biological functions and photocatalytic degradation properties. *LWT- Food Science and Technology*, *134*(April), 110–133.

Shafey, A. M. El. (2020). Green synthesis of metal and metal oxide nanoparticles from plant leaf extracts and their applications: A review. *Green Processing and Synthesis*, *9*(1), 304–339.

Shah, M., Fawcett, D., Sharma, S., Tripathy, S. K., & Poinern, G. E. J. (2015). Green synthesis of metallic nanoparticles via biological entities. *Materials*, *8*(11), 7278–7308.

Sharmila, A. R., & Gayathri, R. Ȧ. (2014). Green Synthesis of Zinc Oxide Nanoparticles by using Hibiscus rosa-sinensis. *International Journal of Current Engineering and Technology*, *4*(4), 2444–2446.

Singh, J., Dutta, T., Kim, K. H., Rawat, M., Samddar, P., & Kumar, P. (2018). "Green" synthesis of metals and their oxide nanoparticles: Applications for environmental remediation. *Journal of Nanobiotechnology*, *16*(1), 1–24.

Singh, R., Dheeraj, B, P., & Sharma, B. (2017). Synthesis , structural and optical properties of Ag doped ZnO nanoparticles with enhanced photocatalytic properties by photo degradation of organic dyes. *Journal of Materials Science: Materials in Electronics*, *28*(0), 5705–5717.

Tahir, K., Nazir, S., Li, B., Khan, A. U., Khan, Z. U. H., Ahmad, A., & Khan, F. U. (2015). An efficient photo catalytic activity of green synthesized silver nanoparticles using Salvadora persica stem extract. *Separation and Purification Technology*, *150*, 316–324.

Tai, B. H., Nhiem, N. X., Quang, T. H., Ngan, N. T. T., Tung, N. H., Kim, Y., Lee, J. J., Myung, C. S., Cuong, N. M., & Kim, Y. H. (2011). A new iridoid and effect on the rat aortic vascular smooth muscle cell proliferation of isolated compounds from Buddleja officinalis. *Bioorganic and Medicinal Chemistry Letters*, *21*(11), 3462–3466.

Talam, S., Karumuri, S. R., & Gunnam, N. (2012). Synthesis, Characterization, and Spectroscopic Properties of ZnO Nanoparticles. *ISRN Nanotechnology*, *2012*, 1–6.

Tang, F., Wang, D., Meng, L., Hong, Z., Tu, W., Cao, Y., Li, L., Ph, D., Ding, F., Liu, B., Wang, M., Xie,

R., Gao, R., Li, X., Chai, C., Wang, S., Gao, Y., Jin, L., Zhang, Y., … Yu, H. (2013). Preliminary Report: Epidemiology of the Avian Influenza A (H7N9) Outbreak in China. *The New England Journal of Medicine*, *370*(6), 1–11.

Umar, H., Kavaz, D., & Rizaner, N. (2019). Biosynthesis of zinc oxide nanoparticles using albizia lebbeck stem bark, and evaluation of its antimicrobial, antioxidant, and cytotoxic activities on human breast cancer cell lines. *International Journal of Nanomedicine*, *14*, 87–100.

Vanaja, M., & Annadurai, G. (2013). Coleus aromaticus leaf extract mediated synthesis of silver nanoparticles and its bactericidal activity. *Applied Nanoscience (Switzerland)*, *3*(3), 217–223.

Varadavenkatesan, T., Lyubchik, E., Pai, S., Pugazhendhi, A., Vinayagam, R., & Selvaraj, R. (2019). Photocatalytic degradation of Rhodamine B by zinc oxide nanoparticles synthesized using the leaf extract of Cyanometra ramiflora. *Journal of Photochemistry and Photobiology B: Biology*, *199*(September), 111621.

Vijayalakshmi, R., & Rajendran, V. (2012). Synthesis and characterization of nano-TiO2 via different methods. *Scholar Research Library*, *4*(2), 1183–1190.

Wijaya, C. J., Ismadji, S., Aparamarta, H. W., & Gunawan, S. (2019). Optimization of cellulose nanocrystals from bamboo shoots using Response Surface Methodology. *Heliyon*, *5*(11), e02807.

Xu, J., Li, L., Yan, Y., Wang, H., Wang, X., Fu, X., & Li, G. (2008). Synthesis and photoluminescence of well-dispersible anatase TiO2 nanoparticles. *Journal of Colloid and Interface Science*, *318*(1), 29–34.

Yadav, T. P., Yadav, R. M., & Singh, D. P. (2012). Mechanical Milling: a Top Down Approach for the Synthesis of Nanomaterials and Nanocomposites. *Nanoscience and Nanotechnology*, *2*(3), 22–48.

Yang, X., Chung, E., Johnston, I., & Ren, G. (2021). Exploitation of Antimicrobial Nanoparticles and Their Applications in Biomedical Engineering. *Journal of Applied Sciences*, *4520*(11).

Yu, J., Baek, M., Chung, H. E., & Choi, S. J. (2011). Effects of physicochemical properties of zinc oxide nanoparticles on cellular uptake. *Journal of Physics: Conference Series*, *304*(1), 324–329.

Zamiri, R., Rebelo, A., Zamiri, G., Adnani, A., Kuashal, A., Belsley, M. S., & Ferreira, J. M. F. (2014). Far-infrared optical constants of ZnO and ZnO/Ag nanostructures. *RSC Advances*, *4*(40), 20902–20908.

Zare, E., Pourseyedi, S., Khatami, M., & Darezereshki, E. (2017). Simple biosynthesis of zinc oxide nanoparticles using nature's source, and it's in vitro bio-activity. *Journal of Molecular Structure*,

1146, 96–103.

Zare, M., Namratha, K., & Byrappa, K. (2018). Green Synthesis and Characterization of ZnO- Ag Nanocomposite by Thymus vulgaris. *International Journal of Scienitific Research in Science and Technology*, *4*(5), 1636–1640.

Zhou, J., Zhao, F., Wang, Y., Zhang, Y., & Lin, Y. (2007). Size-controlled synthesis of ZnO nanoparticles and their photoluminescence properties. *Journal of Luminescence*, *123*, 195–197.

APPENDIXES

Appendix A: Raw materials, chemicals, and reagents

A	*B.polystachya* leaf
B	*B.polystachya* dye
C	Silver nitrate ($AgNO_3$), Zinc acetate ($(Zn(CHOO)_2.2H_2O)$)
D	Chloroform, Hydrochloric Acid, Sulphuric Acid
E	Bromine water, Iron (III) Chloride Hexahydrate, Sodium Hydroxide
F	Dimethyl sulphoxide
G	Nutrient Broth
H	Mueller Hinton Agar

Appendix B: Synthesis route of ZnO NPs and ZnO-Ag NCs

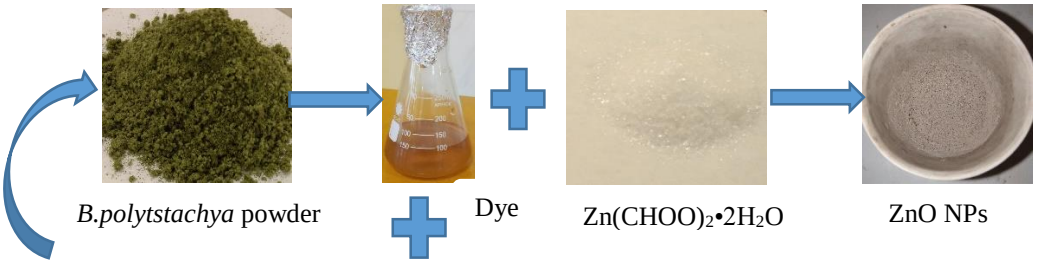

B.polytstachya powder

Dye

$Zn(CHOO)_2•2H_2O$

ZnO NPs

B.polytstachya leaves

$AgNO_3$

$Zn(CHOO)_2•2H_2O$

ZnO-Ag NCs

Appendix C: Supporting pictures during the study

Extraction of the dye from leaf of *B.plystachya*

Filtration of the dye using Whattman no-1filter paper

B.plystachya Leaf extract (dye)

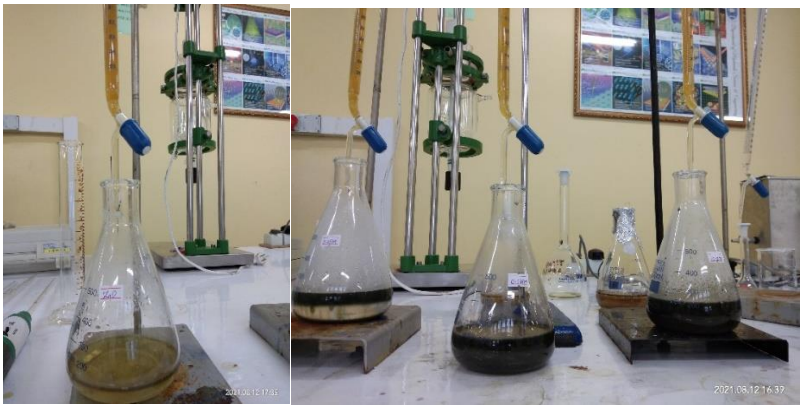

Mixing process of *B.plystachya* leaf extract, zinc acetate dihydrate, and different concentrations of silver nitrate ($AgNO_3$).

pH adjustment of the solutions during synthesis of ZnO Nps and ZnO-Ag NCs

ZnO Nps and ZnO-Ag NCs after centrifugation

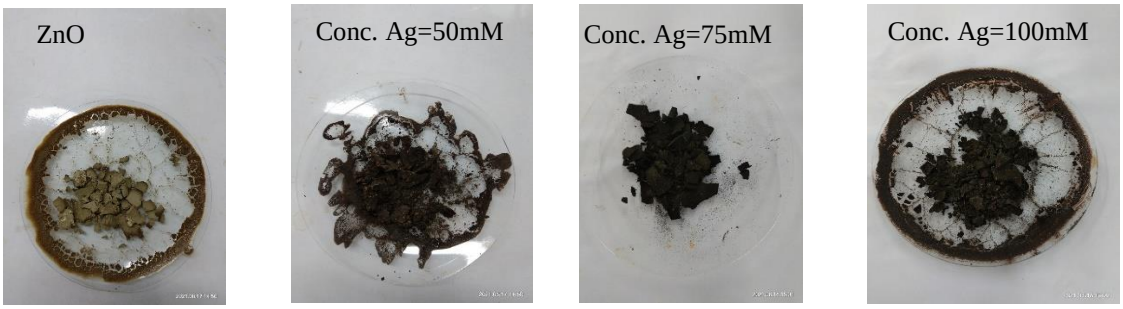

ZnO nanoparticles and ZnO-Ag nanocomposites after oven drying at 105°C

ZnO nanoparticles and ZnO-Ag nanocomposites after calcination at 400°C

Appendix D: Design expert 11 data

Table D1: Fit summary for Absorbance Intensity

Source	Sequential p-value	Lack of Fit p-value	Adjusted R^2	Predicted R^2	
Linear	< 0.0001	0.0004	0.6865	0.6071	
2FI	0.5212	0.0003	0.6736	0.3442	
Quadratic	**< 0.0001**	**0.1214**	**0.9762**	**0.9189**	**Suggested**
Cubic	0.2135	0.1112	0.9830	0.4850	Aliased

Table D2: Diagnostics Case Statistics report for Absorbance Intensity

Run Order	Actual Value	Predicted Value	Residual	Leverage	Internally Studentized Residuals	Externally Studentized Residuals	Cook's Distance	Influence on Fitted Value DFFITS	Standard Order
1	1.76	1.74	0.0191	0.672	0.500	0.481	0.051	0.688	6
2	1.42	1.40	0.0185	0.672	0.484	0.464	0.048	0.664	7
3	1.63	1.61	0.0231	0.166	0.380	0.363	0.003	0.162	18
4	0.7547	0.7714	-0.0167	0.603	-0.398	-0.381	0.024	-0.469	9
5	1.08	1.11	-0.0226	0.672	-0.591	-0.571	0.072	-0.817	4
6	0.6236	0.5697	0.0539	0.672	1.411	1.496	0.408	2.140(1)	1
7	1.73	1.65	0.0750	0.603	1.787	2.055	0.485	2.534(1)	12
8	0.6069	0.5749	0.0320	0.608	0.768	0.751	0.092	0.936	13
9	0.8450	0.8624	-0.0174	0.672	-0.455	-0.437	0.042	-0.625	5
10	1.63	1.61	0.0204	0.166	0.336	0.320	0.002	0.143	20
11	1.10	1.12	-0.0175	0.603	-0.417	-0.399	0.026	-0.491	11

12	0.9563	1.01	-0.0584	0.672	-1.530	-1.659	0.479	-2.373[(1)]	2
13	1.95	2.04	-0.0938	0.672	-2.458	-3.706	1.236[(1)]	-5.302[(1)]	8
14	1.65	1.61	0.0403	0.166	0.663	0.643	0.009	0.287	16
15	1.75	1.67	0.0742	0.603	1.769	2.024	0.475	2.496[(1)]	10
16	1.62	1.61	0.0113	0.166	0.186	0.177	0.001	0.079	15
17	1.59	1.61	-0.0184	0.166	-0.302	-0.288	0.002	-0.129	19
18	0.8450	0.9040	-0.0590	0.672	-1.547	-1.683	0.490	-2.407[(1)]	3
19	1.63	1.60	0.0246	0.608	0.590	0.569	0.054	0.709	14
20	1.52	1.61	-0.0887	0.166	-1.458	-1.559	0.042	-0.696	17

[(1)] Exceeds limits.

Table D$_3$: Sample Sequential Model Sum of Squares for Absorbance Intensity

Source	Sum of Squares	df	Mean Square	F-value	p-value	
Mean vs Total	35.66	1	35.66			
Linear vs Mean	2.61	3	0.8689	14.87	< 0.0001	
2FI vs Linear	0.1441	3	0.0480	0.7892	0.5212	
Quadratic vs 2FI	**0.7466**	**3**	**0.2489**	**56.09**	**< 0.0001**	**Suggested**
Cubic vs Quadratic	0.0254	4	0.0063	2.00	0.2135	Aliased
Residual	0.0190	6	0.0032			
Total	39.20	20	1.96			

Select the highest order polynomial where the additional terms are significant and the model is not aliased.

Contour and 3D plots for insignificant factors

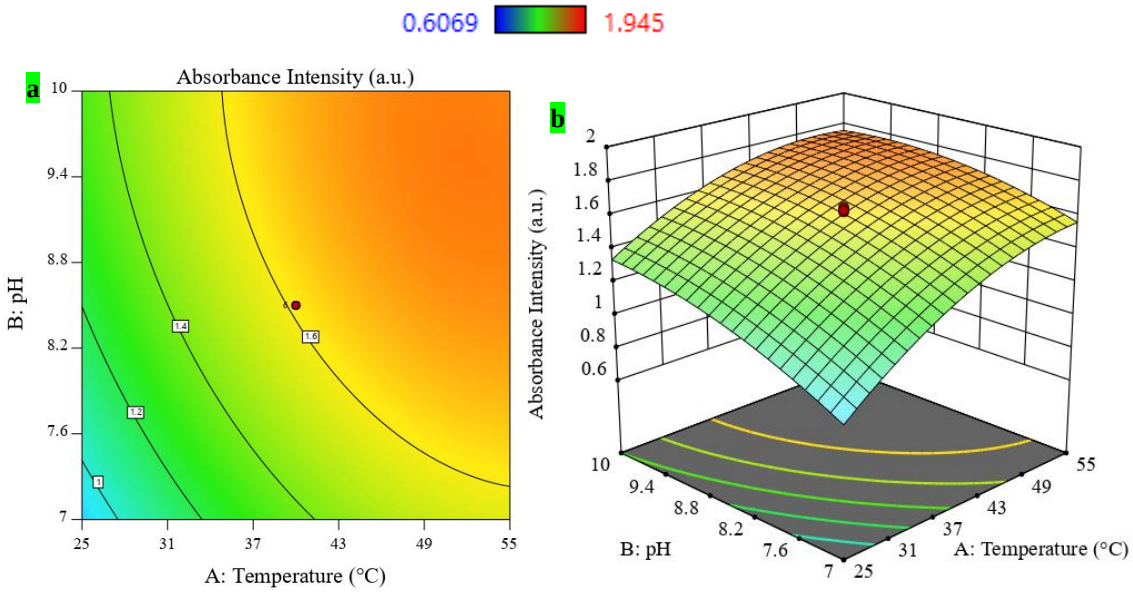

Figure D1: (a) Contour plot and **(b)** 3D response surface plot for Temperature – pH effect on absorbance intensity.

Perturbation graphs

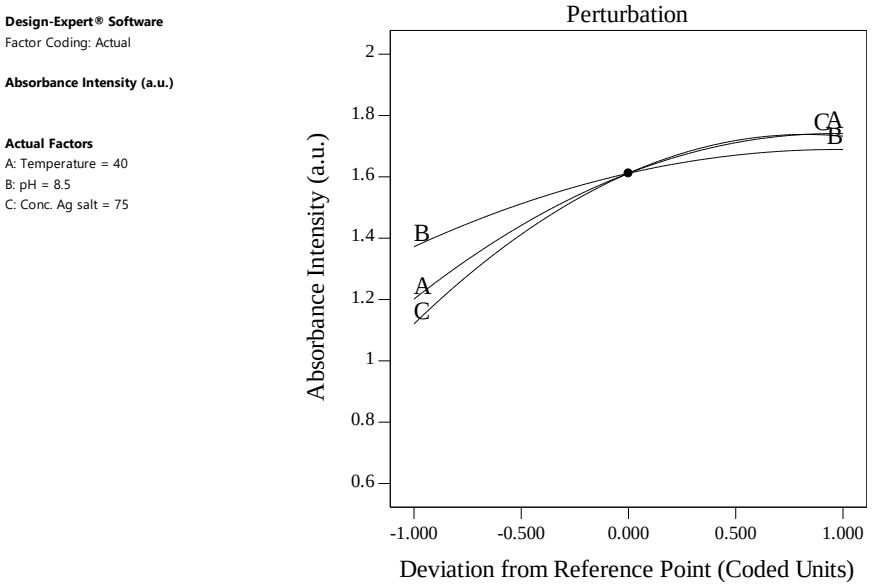

Figure D2: Perturbation graphs of Absorbance Intensity

Cubic diagram

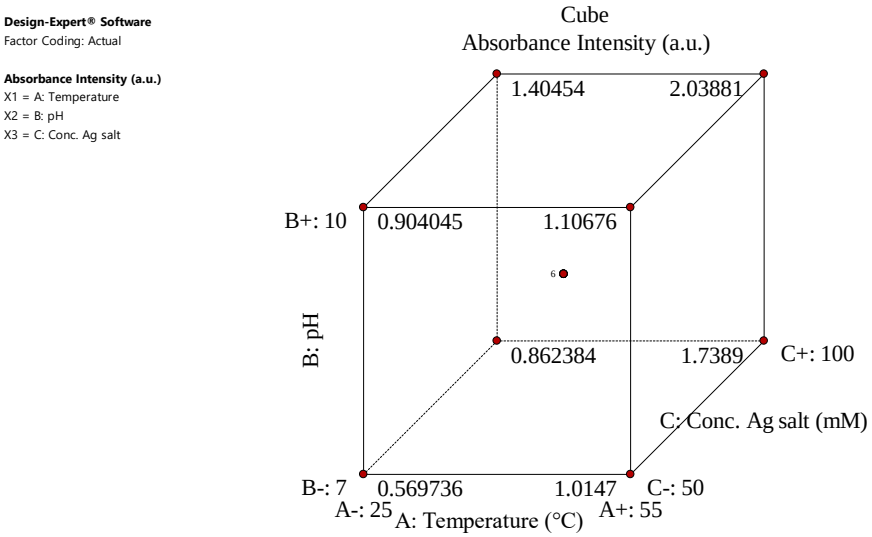

Figure D2: Cubic representation of the process parameters (temp., pH, Conc. Ag salt) and the response (Absorbance intensity)